A Self-Consistent ECRH Ray Tracing Calculation for a Tandem Mirror Transport Code

D.G. Braun and G.A. Emmert

April 1983

UWFDM-502

FUSION TECHNOLOGY INSTITUTE

UNIVERSITY OF WISCONSIN

MADISON WISCONSIN

A Self-Consistent ECRH Ray Tracing Calculation for a Tandem Mirror Transport Code

D.G. Braun and G.A. Emmert

Fusion Technology Institute
University of Wisconsin
1500 Engineering Drive
Madison, WI 53706

http://fti.neep.wisc.edu

April 1983

UWFDM-502

A SELF-CONSISTENT ECRH RAY TRACING CALCULATION FOR A TANDEM MIRROR TRANSPORT CODE

D.G. Braun

G.A. Emmert

Fusion Engineering Program
Nuclear Engineering Department
University of Wisconsin-Madison
Madison, Wisconsin 53706

April 1983

UWFDM-502

Abstract

A mechanism has been developed by which a 3-dimensional ECRH ray tracing-absorption calculation may be coupled to a tandem mirror transport code. The radial temperature and density profiles of the transport code are expanded via flux conservation to provide the 3-dimensional geometry required for the ray tracing calculation. Absorption along the ray trajectory determines an equivalent radial ECRH power deposition profile for use by the transport code. Singularities in this profile that are created by using a single ray to model an ECRH system with broad spatial heating are discussed, as well as their removal using multiple rays. A technique for artificially producing these multiple ray simulations will be presented and compared with results where multiple ray tracing calculations were performed. Examples of plasma buildup simulations for a tandem mirror using ECRH in the plug are provided, where the results of this work have been used to self-consistently couple the plasma profiles and the power absorption. A positive feedback mechanism is identified which produces locally large electron temperatures when ECRH power deposition is greater than the electron energy losses in a radial transport zone. This mechanism frequently occurs near the plasma edge, shielding the electrons near the plasma axis from launched ECRH power, and producing a hollow temperature profile. This may lead to the collapse of the plug plasma.

I. Introduction

A significant improvement in tandem mirror performance is expected by the addition of thermal barriers, which are regions of reduced electrostatic potential between the central cell and plug; the lower potential reduces the communication between the plug and central cell electrons. The lower thermal contact between the two species allows the plug electrons to be efficiently heated, maintaining a higher temperature than the central cell electrons. This creates an increased plasma plug potential that axially confines the central cell ions.

Electron Cyclotron Resonance Heating (ECRH) has two possible uses in the thermal barrier concept. It can be used to heat the plug electrons to their higher temperature, and can be used to create a species of hot magnetically confined electrons at the barrier minimum. The trapping of these electrons further enhances the potential dip there. Future experiments will test the ability of ECRH to maintain barrier and plug electron species in a thermal barrier configuration,[1,2] and tandem mirror reactor studies have been performed which rely on these ECRH heated electrons to provide the high performance needed for economic feasibility.[3,4]

To study the spatial variation of ECRH heating in an inhomogeneous plasma, Audenaerde has written a 3-dimensional code to model the heating process.[5] Ray trajectories through the plasma are calculated using the equations of geometric optics, and power deposition is determined by treating the plasma as a dielectric and calculating its absorptivity. His results indicate a strong variation in both the degree of wave absorption and its spatial location, depending upon such factors as the wave mode (ordinary vs.

extraordinary), plasma density, electron temperature and the angle of propagation relative to the magnetic field lines.

The modeling of an ECRH heated plasma requires an accurate treatment of the power deposition. The changing electron temperature and density, especially in the case of plasma buildup, will alter the magnitude of the absorption and often change its spatial location. The power deposited will then in turn affect the evolution of the plasma parameters. In order to accurately model ECRH heating of a tandem mirror plasma we have developed a technique for coupling the 3-dimensional ray tracing-absorption calculation of Audenaerde to a tandem mirror radial transport code.

A transport code models a tandem mirror plasma by solving fluid equations in cylindrical geometry. Axial variations are ignored and the plasma is assumed to be confined in a magnetic square well of length L. Azimuthal symmetry is also assumed so that solving the fluid equations yields radial profiles of the temperature and density. The nonaxisymmetric effects on transport are included by using modified radial diffusion coefficients.[6] The particle end-loss from the mirror cells is simulated by using analytic expressions for the effective axial loss times.[7,8] Neutral beam particle and energy deposition, as well as any RF heating of particles are modeled by adding source terms to the equations governing each radial zone's temperature and density.

The assumption of axial and azimuthal symmetry and the division of the plasma into finite radial zones of uniform density and temperature is consistent with particle motion in a tandem mirror. A particle confined in a mirror will have an axial bounce time that is much smaller than any transport time scale. Also, a trapped particle will have a guiding center drift given by

$$\vec{V}_{drift} = \frac{\vec{E} \times \vec{B}}{B^2} - \frac{1}{q}\frac{\mu}{B^3}\vec{B} \times \vec{\nabla}\frac{B^2}{2} + \frac{mv_{\parallel}^2}{qB^2}\frac{\vec{R}_c \times \vec{B}}{R_c^2}$$

where $\vec{E}$ is the electric field produced by the plasma potential, q is the particle charge, μ is the particle's magnetic moment, R_c is the magnetic field's radius of curvature, and $\vec{B}$ is the magnetic field. The radial density profile produces a radial electrostatic potential variation which, together with the radial variation of B^2 creates an azimuthal drift of particles on a flux surface. Particles and energy deposited locally will be azimuthally spread on a time scale faster than that of radial transport, so that particle temperatures and densities will be constant on a flux surface.

The coupling mechanism we have developed creates the 3-dimensional density and temperature models required for the ray tracing calculation by extending the radial plasma profiles of a transport code along these flux surfaces. The power absorbed is calculated per unit length along the ray's trajectory. The energy deposited in a radial transport zone when it is traversed by the ECRH ray is then averaged over the entire zone to produce the power source used in the transport code's fluid equations. In this way we model the locally heated electron which azimuthally drifts as it bounces in the mirror trap sharing its energy with the other electrons on its flux surface. By incorporating the ray tracing calculation in this way, the ECRH power deposition radial profile produced for use by the transport code in its subsequent time evolution of the plasma is assured of being self-consistent with the current plasma parameters.

The coupling mechanism developed to line the ray tracing-absorption calculation to a transport code is discussed in Section II of this report. When using a single ray to model the finite spot size of the incident micro-

wave power, singularities will be created in the power deposited per electron. This phenomena and the need to use multiple ray simulations of the incident power are discussed in Section III. We use these results to couple an ECRH power deposition calculation as a subroutine to the TAMBAR[9] transport code, and in Section IV we illustrate its use by analyzing the startup scenario for the materials engineering test facility, TASKA.[4] These simulations show the effect ECRH heating may have on plasma evolution and illustrate the need for self-consistent calculations. In Section V we summarize our work.

II. The Coupling Mechanism

The ray tracing code of Audenaerde[5] employed here uses the equations of geometrical optics to calculate a ray trajectory through a plasma in a fully 3-dimensional, (x,y,z) geometry. The wave path is determined as a sequence of points separated by a distance calculated from a fixed time increment and the wave's group velocity. At each of these points the propagation direction, $\vec{k}$, is reevaluated and the plasma absorptivity, α, is calculated. The unabsorbed power in the ray along its trajectory is given by the equation,

$$P(x,y,z) = P_o e^{-\int \alpha(x,y,z) ds} \qquad (1)$$

where the integral is evaluated along the ray trajectory and P_o is the initial power. To perform this calculation the ray tracing code requires at any (x,y,z) point the values of:

electron temperature, $T_e(x,y,z)$

plasma density, $n(x,y,z)$

magnetic field, $\vec{B}(x,y,z)$

magnetic field gradient, $\vec{\nabla}B(x,y,z)$

plasma density gradient, $\vec{\nabla}n(x,y,z)$.

The two gradients are required for the geometrical optics calculation. The vacuum magnetic field and its gradient are provided by analytic expressions that closely approximate the true field. Thus, the coupling mechanism used must provide an accurate 3-dimensional model of the electron temperature, the plasma density and its gradient from the 1-dimensional transport code's radial profiles.

The method used employs flux conservation to determine the 3-dimensional flux surfaces. We will assume that the electron temperature is constant on these surfaces, and that the plasma density varies only axially as a result of variations in the magnetic field and plasma potential. Choosing our coordinates so that the z-axis is along the magnetic axis of the tandem mirror, we can trace out these flux surfaces if we assume that the cross-sections of the surfaces in the plane perpendicular to the z-axis are ellipses, all of the same ellipticity (see Fig. 1). The flux tube is then determined by the varying ellipticity and magnitude of B(z) along the z-axis; this dependence can be determined a priori from the magnetic field configuration.

Using the equation of an ellipse,

$$\frac{x^2}{a^2(z)} + \frac{y^2}{b^2(z)} = 1 \ , \tag{2}$$

the definition of the ellipticity ϵ,

$$\epsilon(z) = \frac{a(z)}{b(z)} \ , \tag{3}$$

Fig. 1

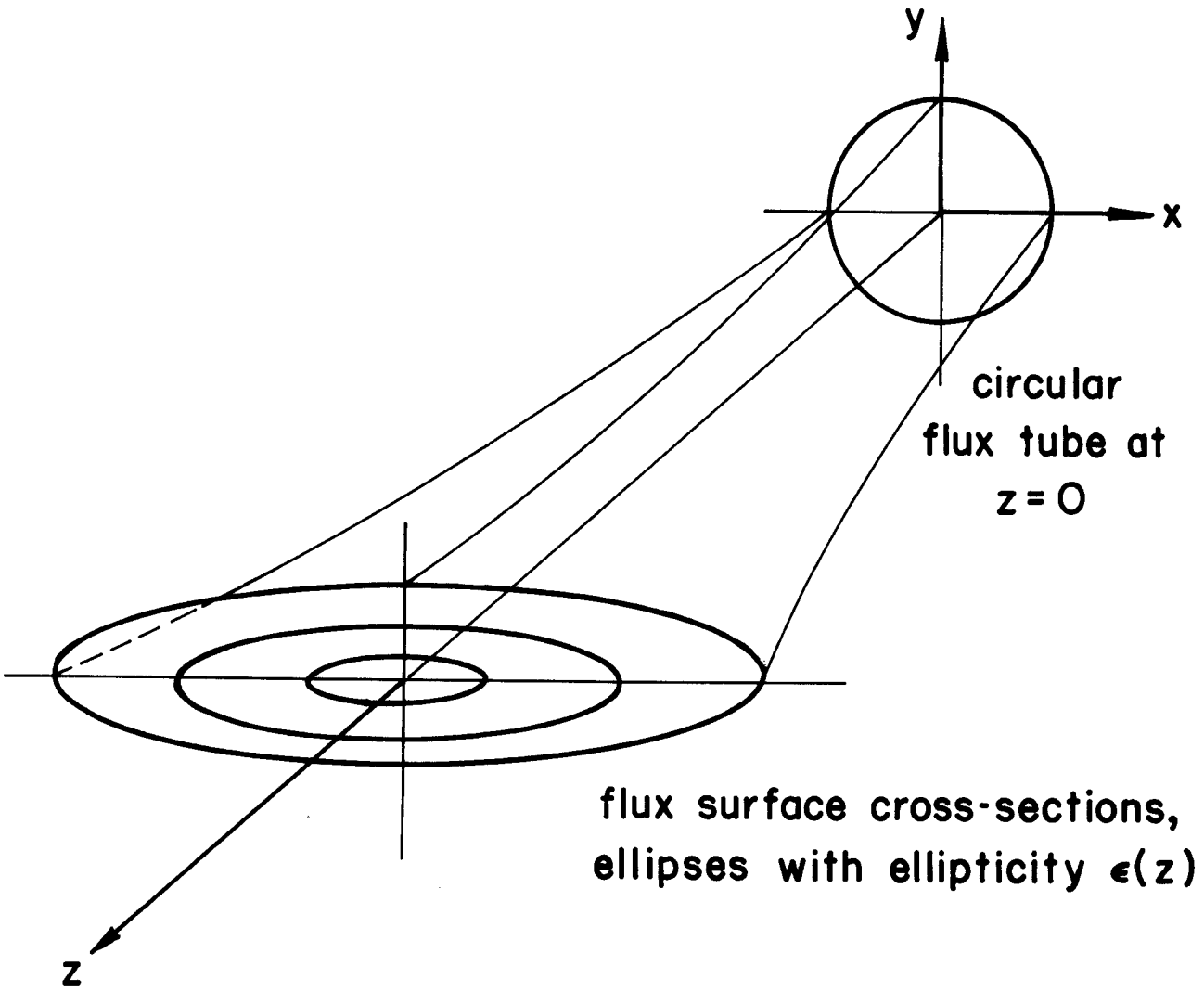

FIGURE 1: FLUX SURFACES ALONG A MAGNETIC AXIS WHOSE CROSS - SECTIONS VARY AXIALLY.

and conservation of magnetic flux,

$$\pi a(z)b(z)B(z) = \text{constant} , \tag{4}$$

the equation of a flux surface can be written as

$$x^2 + \varepsilon^2(z)y^2 = \frac{\varepsilon(z)B(0)}{B(z)} r^2 . \tag{5}$$

Here B(0) is the magnetic field at z = 0 where the flux surface is assumed to be circular with radius r. The magnetic field B(z) is assumed to be uniform over the cross-section of the ellipse at any z under consideration.

For any (x,y,z) point at which the ray tracing calculation requires plasma parameters, we use Eq. (5), together with the known ellipticity $\varepsilon(z)$, to determine the midplane radius, r, which is the coordinate used in the transport code. Using this radius the electron temperature at the point can be determined from the transport code radial profile data. These points are fit with a Chebyshev polynomial expansion, so that the electron temperature can be evaluated at any value of radius r. In a similar manner the plasma density on the flux surface at z = 0 can be evaluated. An axial variation of the density on a flux surface must be assumed to determine the value of the density at the (x,y,z) point in question. This axial variation depends, of course, on the actual plasma configuration being modeled.

The last piece of information required for the execution of the ray tracing calculation is the evaluation of the density gradient. This can be obtained by writing the equation of a flux surface as

$$\frac{B(z)}{B(0)}\left(\frac{x^2}{\varepsilon(z)} + \varepsilon(z)y^2\right) = \text{constant} = r^2 \tag{6}$$

where r is the radius of the flux surface at z = 0. We then let

$$n(x,y,z) = g(r)h(z) \tag{7}$$

where h(z) allows for the axial density variation (with h(0) = 1) and g(r) is the fitted polynomial expansion describing the density profile at z = 0. Then

$$\vec{\nabla}n = h\frac{\partial g}{\partial r}\vec{\nabla}r + g\frac{\partial h}{\partial z}\hat{z} \tag{8}$$

where $\vec{\nabla}r$ is computed explicitly from Eq. (6), h and $\partial h/\partial z$ are assumed given as functions of z, and q and $\partial q/\partial r$ are obtained from the transport code. Physically, the first term in Eq. (8) represents the normal gradient on the flux surface, while the second term is of course the contribution from the assumed axial density variation.

Using this mapping, we have written the ray tracing-absorption calculation as a subroutine of a transport code. When called, the radial profiles of the plasma density and electron temperature are transferred to a subroutine where the above analysis is used to create 3-dimensional models for the ray tracing calculation. Absorption calculations provide the beam attenuation at the (x,y,z) points along the ray's path. Through our coupling mechanism these points are mapped into the equivalent radii of the transport code's circular geometry, so that the power deposition in each of the radial transport zones may then be determined. Dividing this by the total number of electrons in each zone yields the averaged energy deposition per electron, which appears as

a source term in the fluid equation describing the electron temperature evolution. Calling this subroutine every few time steps during a plasma simulation will insure that the ECRH absorption profiles used by the transport code are always self-consistent with the temperature and density profiles.

III. Singularities Produced in Single Ray Simulations

The use of a single ray to model an ECRH heating system assumes that the entire antenna power is concentrated in an infinitesimally thin pencil beam along the ray's path. In reality, an antenna will launch power over a range of angles producing a spread in the spatial heating. The use of multiple sources will produce further spatial spreading of ECRH power, both effects resulting in a spot size on the plasma analogous to the footprint of neutral beams. When using a single ray to simulate a heating system, singularities in the power deposition will result from the full power pencil beam assumption and the finite radial zones of the transport code.

There are two types of singularities which arise when using a pencil beam model incident on a cylindrical plasma. The first occurs when the beam passes through the plasma axis; this is beam A of Fig. 2. For a cylinder of radius r centered on the axis, the beam power absorbed will be proportional to the ray's path length through the cylinder, 2r, while the number of electrons in the cylinder is proportional to r^2. Thus, for such a beam the power deposited per electron in the cylinder is

$$\frac{\text{Power absorbed}}{\text{\# electrons}} \propto \frac{1}{r} \tag{9}$$

so that power deposition per electron becomes infinite as the cylinder's volume is decreased.

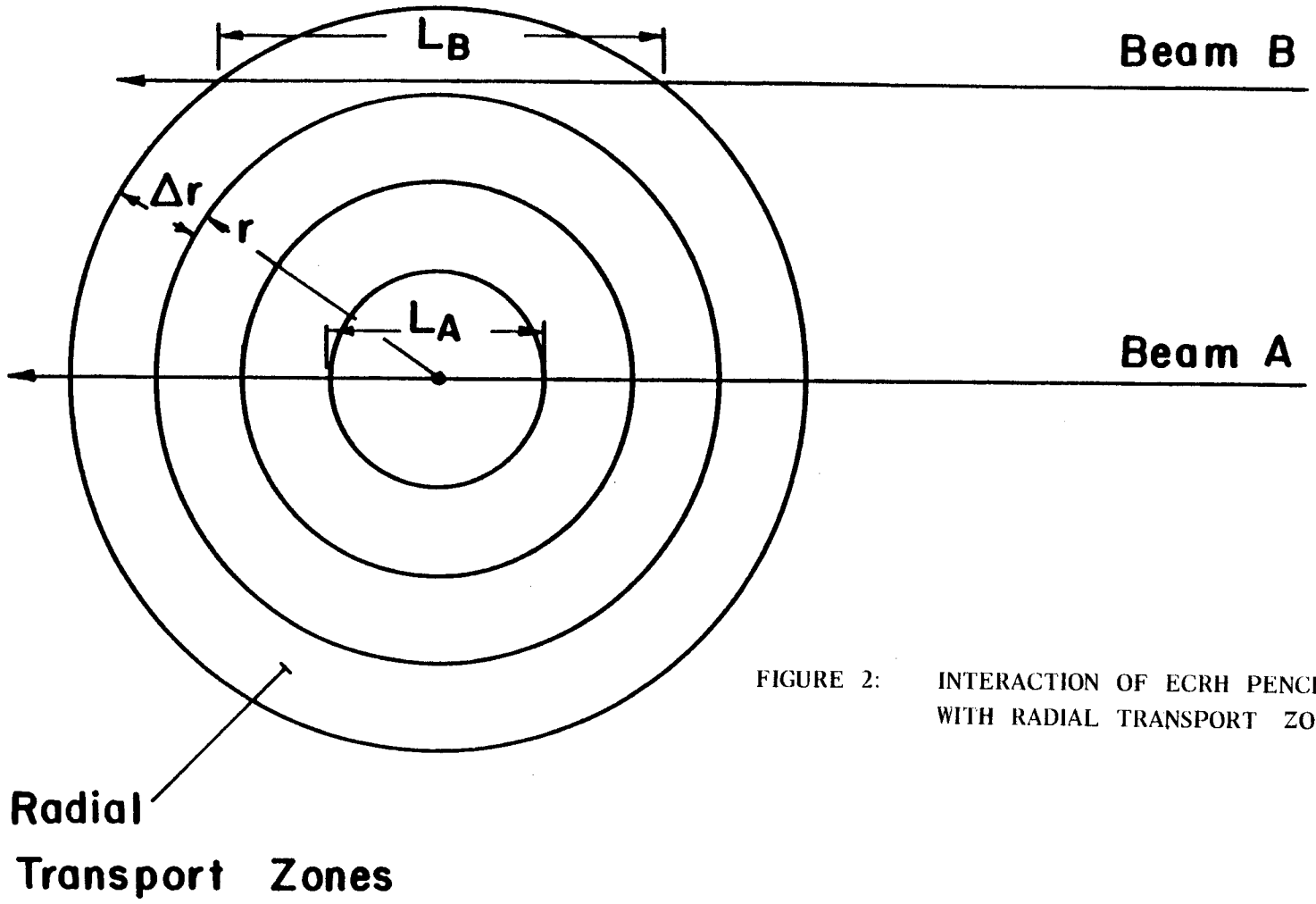

FIGURE 2: INTERACTION OF ECRH PENCIL BEAMS WITH RADIAL TRANSPORT ZONES

A second type of singularity occurs when the ray is tangent to a cylindrical surface, as is beam B of Fig. 2. In this case the ray's path length through the annular zone of thickness Δr is given by

$$L = 2[(r + \Delta r)^2 - r^2]^{1/2} \cong 2[2r\Delta r]^{1/2} \ . \tag{10}$$

The power deposited per electron in an annular zone of length L_{zone} is then

$$\frac{\text{power absorbed}}{\text{\# electrons}} \cong \frac{P_o \alpha 2(2r\Delta r)^{1/2}}{n\ 2\pi r \Delta r L_{zone}} \propto \frac{1}{\sqrt{\Delta r}} \tag{11}$$

and again a singularity is produced, the magnitude of which depends on the zone size. Both types of singularities will arise if we couple a single ray model for ECRH to a transport code, where the zonal size is kept small to increase accuracy.

Each of these singularities is created by the assumption of a pencil beam for the ECRH, where the entire system's power is concentrated along the ray's path and the energy deposited is roughly proportional to the path length through the zone. In the above examples the volume of the zones decreased faster than the path lengths so that the singularities resulted. In reality, only a fraction of an antenna's power will in fact traverse the finite size transport zones, and heating in the zones will be described by a ray whose power is determined by comparing the zone's cross-sectional area normal to the ray and the finite size ECRH spot. With the ECRH power accessible to a zone now dependent upon the zone's size, the power deposited per electron becomes independent of the size of the transport zone.

For the on-axis singularity, the first case considered above, a cylinder of radius r will show to an incident normal ray a heating surface proportional to its thickness, 2r. The ray heating this cylinder will not, as assumed before, have a power level equal to that of the entire ECRH system, P_o, but rather will be proportional to the heating area surface, P_oCr, where C represents some shape factor. Equation (9) will then be modified so that the power deposited per electron in a cylinder of length L_{zone} is

$$\frac{\text{(Power in ray)(fraction absorbed)}}{\text{\# electrons}} = \frac{(P_oCr)(\alpha\ 2r)}{n\pi r^2 L_{zone}} = \text{constant}$$

and we see there is in fact no singularity.

The second singularity discussed, when a full power ray is tangent to a cylindrical surface, also disappears when the power in the ray is made proportional to the zone's heating cross-section. With a full power ray transitting an annular zone of thickness Δr, the power deposited per electron was found to be proportional to $\Delta r^{-1/2}$. If as above, we assume the power in the tangent ray is proportional to the zone's incident thickness, Δr, then the power per electron will go as $\Delta r^{1/2}$ and approach zero instead of infinity as the zone thickness decreases. Physically, this says that a tangent ray cannot deposit enough energy by itself to heat an annular region of electrons. When the energy from all rays incident on the annulus is considered, the power per electron is as expected, a constant independent of Δr.

To illustrate this we consider a ray representing the fraction of the total system power in the strip of width dy incident on the annular region at height y, as shown in Fig. 3. As before, we will assume the power level to be given by $P_oC\ dy$. The path length through the annulus at height y is

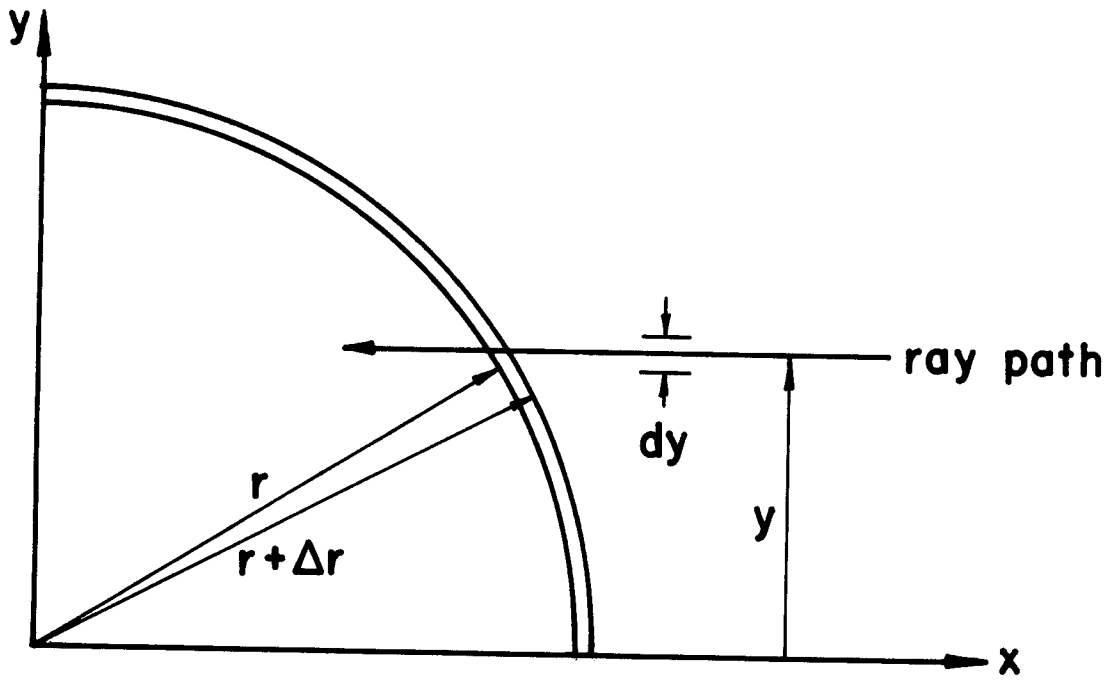

FIGURE 3: AN ECRH RAY AT HEIGHT **y** AND WITH THICKNESS **dy** TRANSVERSING A SHELL OF THICKNESS **Δr** AT RADIUS **r**.

$$L = [(r + \Delta r)^2 - y^2]^{1/2} - [r^2 - y^2]^{1/2}$$

which is the generalized form of Eq. (10). The power deposited in the annulus by this ray is then

$$dP = (P_0 C\ dy)\alpha\ \{[(r + \Delta r)^2 - y^2]^{1/2} - [r^2 - y^2]^{1/2}\}\ .$$

We now sum over all rays contributing by integrating from y = 0 to y = r, and assume symmetry so that the four quadrants of the annulus have equal power absorption. If the factor $P_0 C\alpha$ can be assumed constant, the integral can be evaluated directly as

$$\text{Power} = 4\ P_0 C\alpha \int_0^r dy\ \{[(r + \Delta r)^2 - y^2]^{1/2} - [r^2 - y^2]^{1/2}\} \tag{12}$$

$$= 2\ P_0 C\alpha\ [r(2r\Delta r + \Delta r^2\ )^{1/2} + (r + \Delta r)^2 \sin^{-1}\ (\frac{r}{r + \Delta r}) - r^2\ \frac{\pi}{2}]\ .$$

Keeping only terms to first order in $\Delta r/r$ and using the expansion[10]

$$\sin^{-1}(1 - z) = \frac{\pi}{2} - (2z)^{1/2}[1 + \sum_{k=1}^{\infty} \frac{1 \cdot 3 \cdot 5 \ldots (2k - 1)}{2^{2k}(2k + 1)k!}\ z^k]$$

we find

$$\text{Power} = 2\pi P_0 C\alpha r\Delta r$$

so that the power deposited per electron in the annulus is

$$\frac{\text{Power from all rays}}{\text{\# electrons}} = \frac{2P_0 C\alpha r\ \Delta r}{n\ 2\pi r\ \Delta r\ L_{zone}} = \frac{P_0 C\alpha}{nL_{zone}} = \text{constant} .$$

Again we see that the singularity is only a result of the single ray model and disappears in a detailed analysis.

We will illustrate the singularity produced by a single ray simulation using examples taken from the analysis of the ECRH used in the TASKA design. This machine creates a thermal barrier in a mirror cell between the central cell and plug, electrostatically separating those regions' electrons. The ECRH power is applied at the 2 Tesla point on the barrier side of the rising plug magnetic field; the ECRH power heats the trapped plug electrons. The axial profiles of the vacuum magnetic field and plasma potential in the end cells of TASKA are shown in Fig. 4, and a further description of the machine is given in Section IV. The heating system uses a circular array of gyrotrons and reflectors which focus power onto a 26 cm diameter spot centered on the plasma axis. Ordinary wave mode heating is used. The system used is shown in Fig. 5.

The ECRH system is focused to heat along the elliptical plasma's major axis. At the 2 Tesla point flux conservation will map the circular surfaces at the plug midplane into an ellipse with minor axis intercepts at y = b given by

$$\pi r^2 B(0) = \pi b^2 [\varepsilon B]_{2\ \text{Tesla}} .$$

Using the plug midplane vacuum field at 4 Tesla and with an ellipticity of 1.75 at the heating point implies that the plasma boundary, at r = 30 cm in the plug, will map into a minor axis boundary of 32 cm at the 2 Tesla point. Further, the 2 cm thick radial zones of the transport code will be 2.1 cm wide

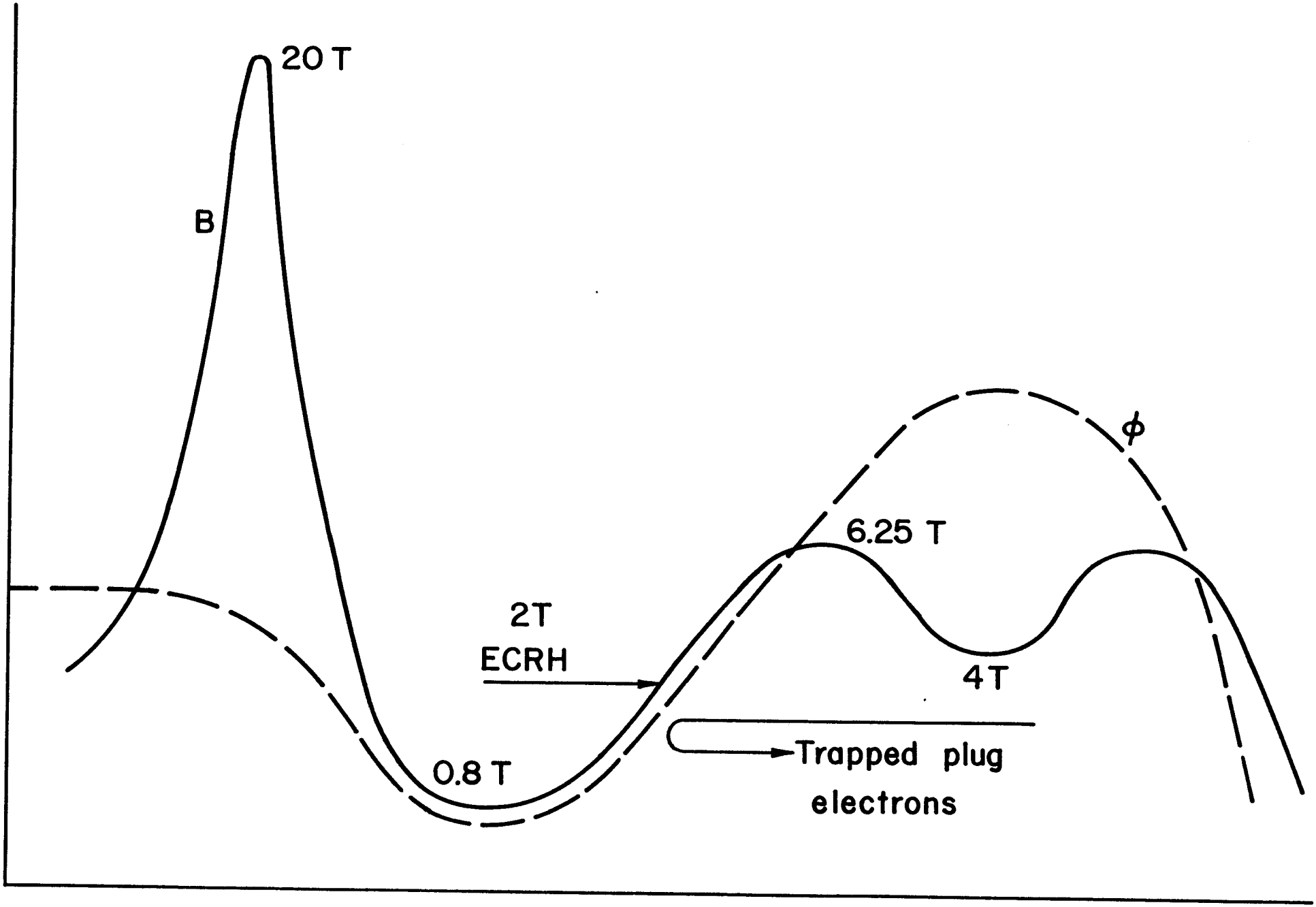

FIGURE 4: ECRH IN TASKA END PLUGS

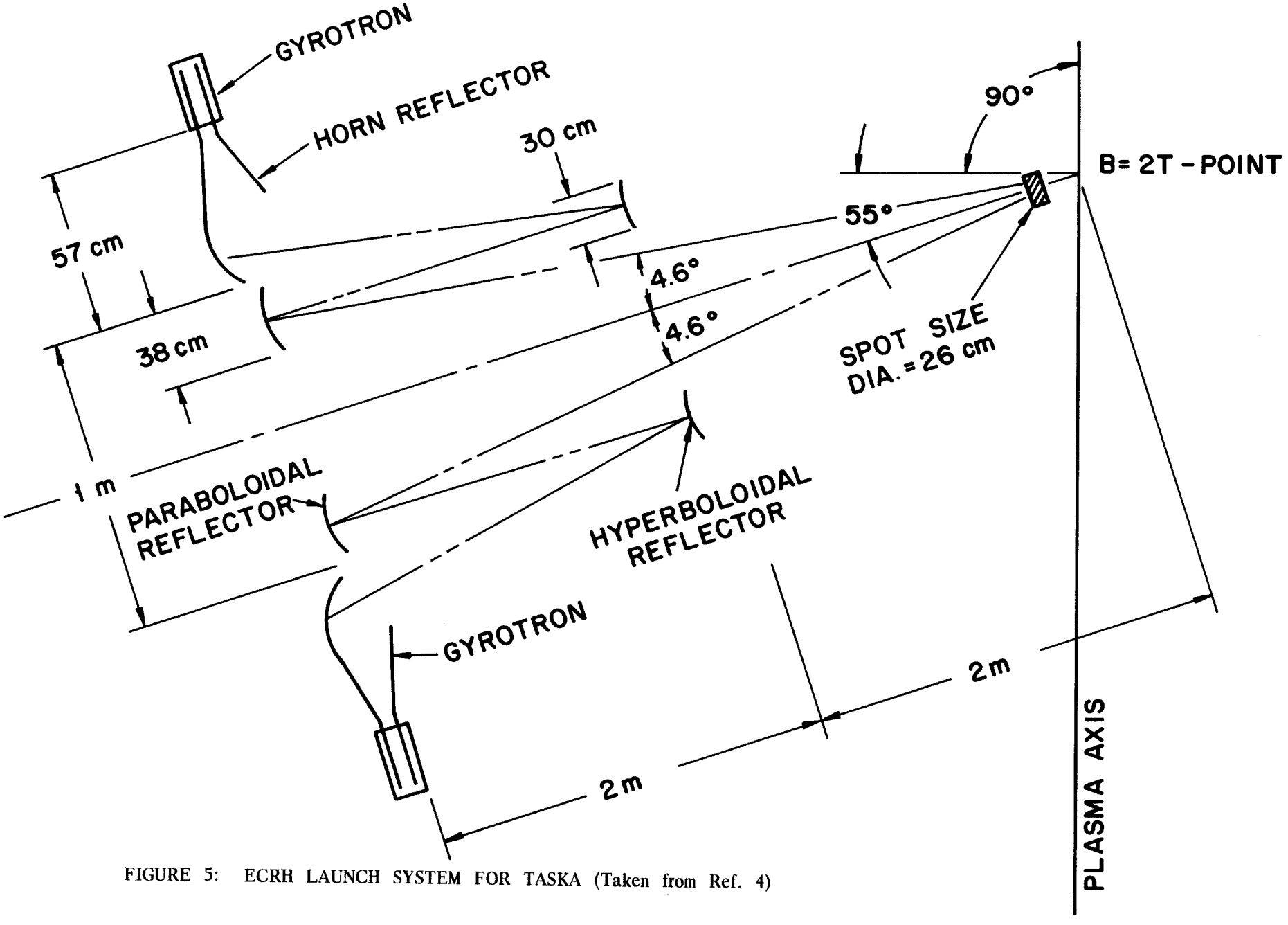

FIGURE 5: ECRH LAUNCH SYSTEM FOR TASKA (Taken from Ref. 4)

along the minor axis. From this we see that a heating system with ECHR power delivered in a 13 cm radius spot will deposit energy over a region large compared to a transport zone. Thus, we anticipate modeling heating by using a single ray centered on the plasma axis will be a poor approximation, and we expect to see the on-axis type singularity in the power deposition profile.

Using typical density and temperature profiles taken from transport code simulations (Gaussians at $n_p \cong 2 \times 10^{13}$ cm^{-3}, $T_{ep} \cong 10$ keV) and using the mechanism of Section II to run the ray tracing-absorption calculation, we simulate the ECRH heating of plug electrons in TASKA. Figure 6 shows the ordinary mode ray trajectory through the plasma using the launch point and angle specified in the TASKA report. In the analysis of plasma startup presented in Section IV this will be one of the two launched points used. Figure 7 shows the fraction of the total system's power deposited per electron as a function of the plug radius that is produced using the single ray heating model. We note the presence of the expected 1/r singularity, and the resulting factor of 20 between the heating rates of on-axis electrons and the main bulk of electrons.

We now model the ECRH heating system by dividing the spot size into horizontal strips, as in Fig. 8, and using a separate ray launched from the center of each strip to simulate the deposition of that strip's power. We assume the launched power is distributed uniformly over the spot, so that the power in each of the horizontal strips is proportional to its fractional area, the product of their width and chord length. Because the heating system and plasma geometry are symmetric in $\hat{y}$, we only need to calculate absorption for rays launched representing strips in the upper half of the spot. Using the same plasma conditions as before, we now calculate the power deposition using

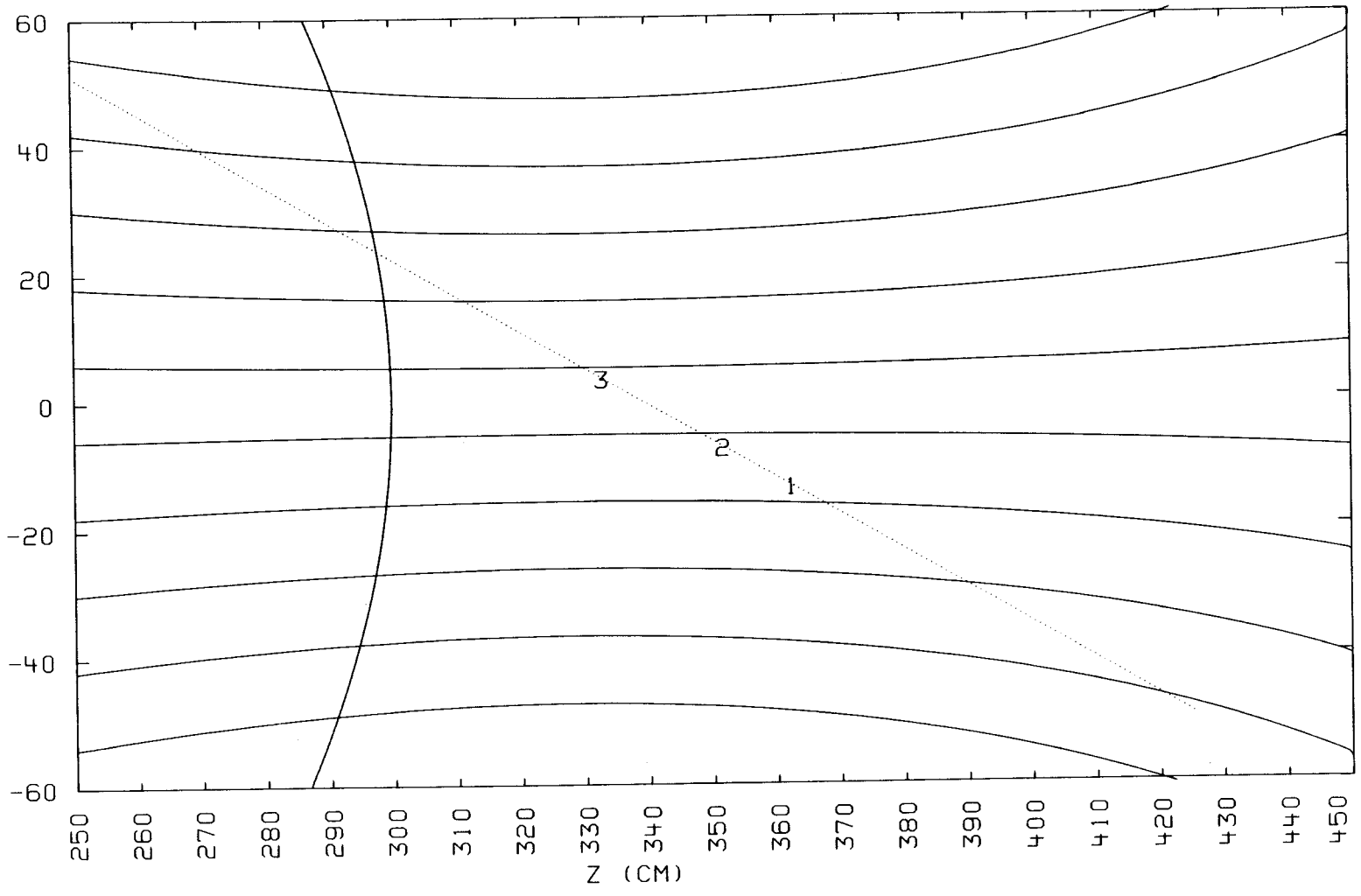

Fig. 6. The ray trajectory for the TASKA design launch through a plasma with an electron temperature of 10 keV and a density of 2×10^{13} cm^{-3}. Shown are magnetic field lines and the 2 Tesla resonance. Absorption along the trajectory is denoted by: 1 = 25%, 2 = 50%, 3 = 75%, and 4 = 99.9% power absorbed.

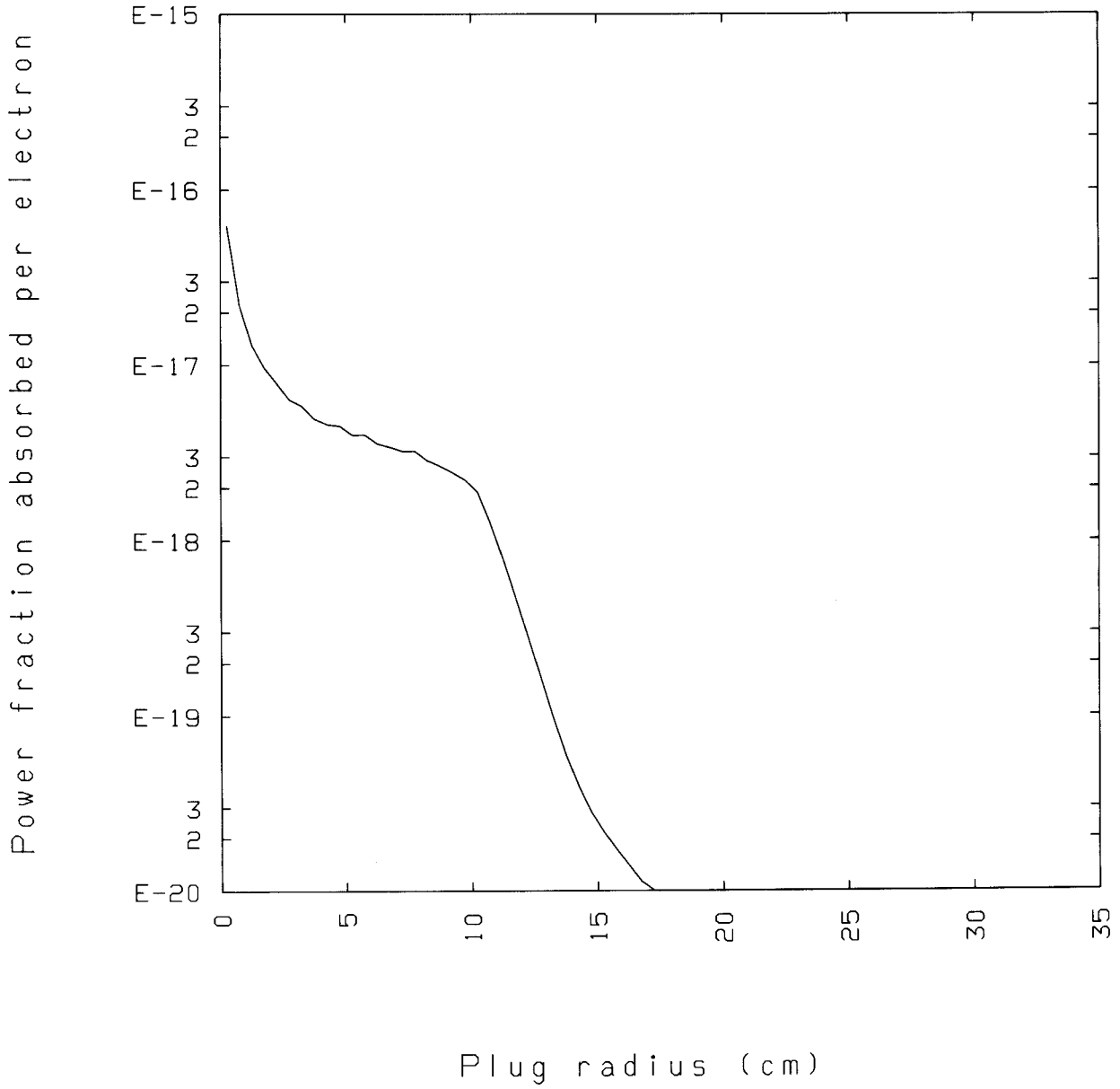

Fig. 7. The fraction of ECRH power absorbed per electron as a function of plug radius using one ray, centered on the plasma axis, to model the plug electron heating in TASKA.

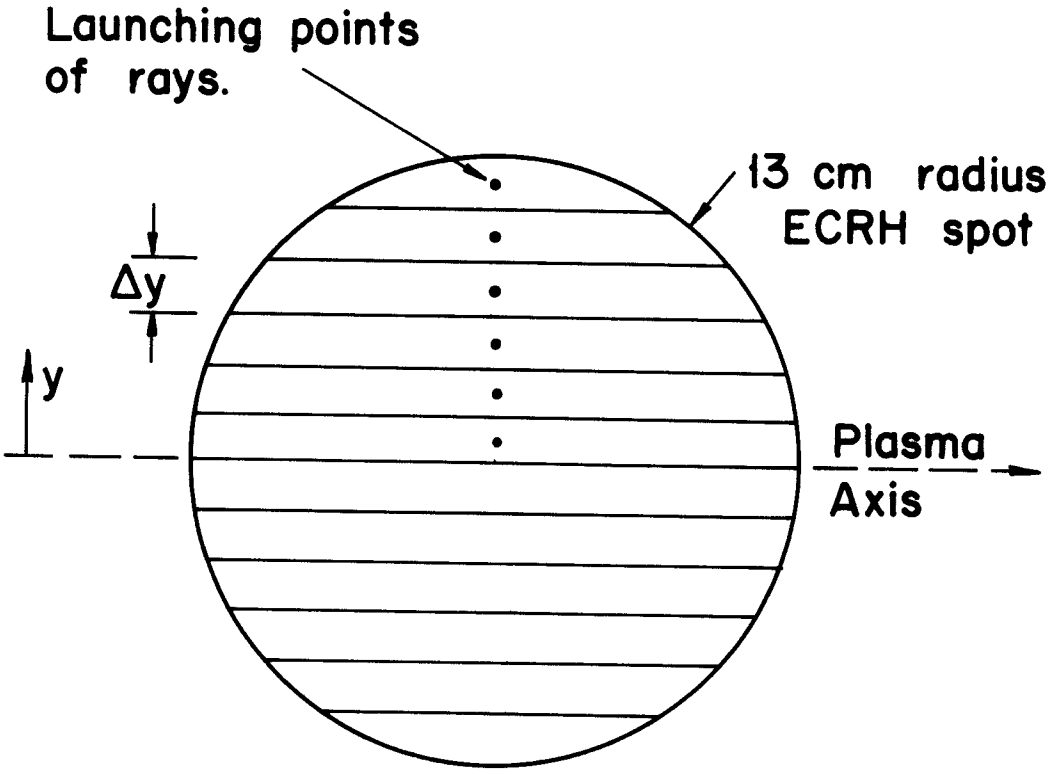

FIGURE 8: MODELLING A CIRCULAR ECRH SPOT USING MULTIPLE RAYS, EACH REPRESENTING THE POWER DEPOSITION FROM A HORIZONTAL STRIP.

26 (52 total) horizontal strips. The resulting power fraction deposited per electron as a function of radius is shown in Fig. 9. We note that the singularity is removed and a flattened power deposition profile is produced, much like the effect of a neutral beam "footprint." By comparing Figs. 7 and 9 the need to use an analysis that correctly models the finite spot size of ECRH systems is apparent, as a power deposition profile with a single ray singularity will create grossly inaccurate temperature profiles.

Since a transport code would make frequent calls to a subroutine calculating ECRH power deposition, it is desirable to make the subroutine's computing time as small as possible. The ray tracing calculations constitute the majority of the subroutine's computations, so we wish to model a finite ECRH spot with as few horizontal strips as possible. In Fig. 10 we show the results of using 6 (12) horizontal strips to model the same absorption calculation as before, where the absorbed power fraction per electron is plotted for each of the radial zones in the transport code. We see that the power deposition profile produced using 6 strips accurately reproduces the more detailed calculation in Fig. 9. Attempts to use fewer than 6 strips will introduce error into the deposition profile, since in those calculations the launched rays now represent strips that are large compared to the width of the transport code's radial zones. Each of the rays will then begin to exhibit singularities in their own absorption, and will combine to produce an inaccurate total absorption profile.

In order to further reduce the computer time required for the ECRH power deposition subroutine, we have developed a technique by which multiple ray trajectories, and the ECRH absorption along them, may be accurately constructed from only one ray tracing calculation. The individual 3-dimensional

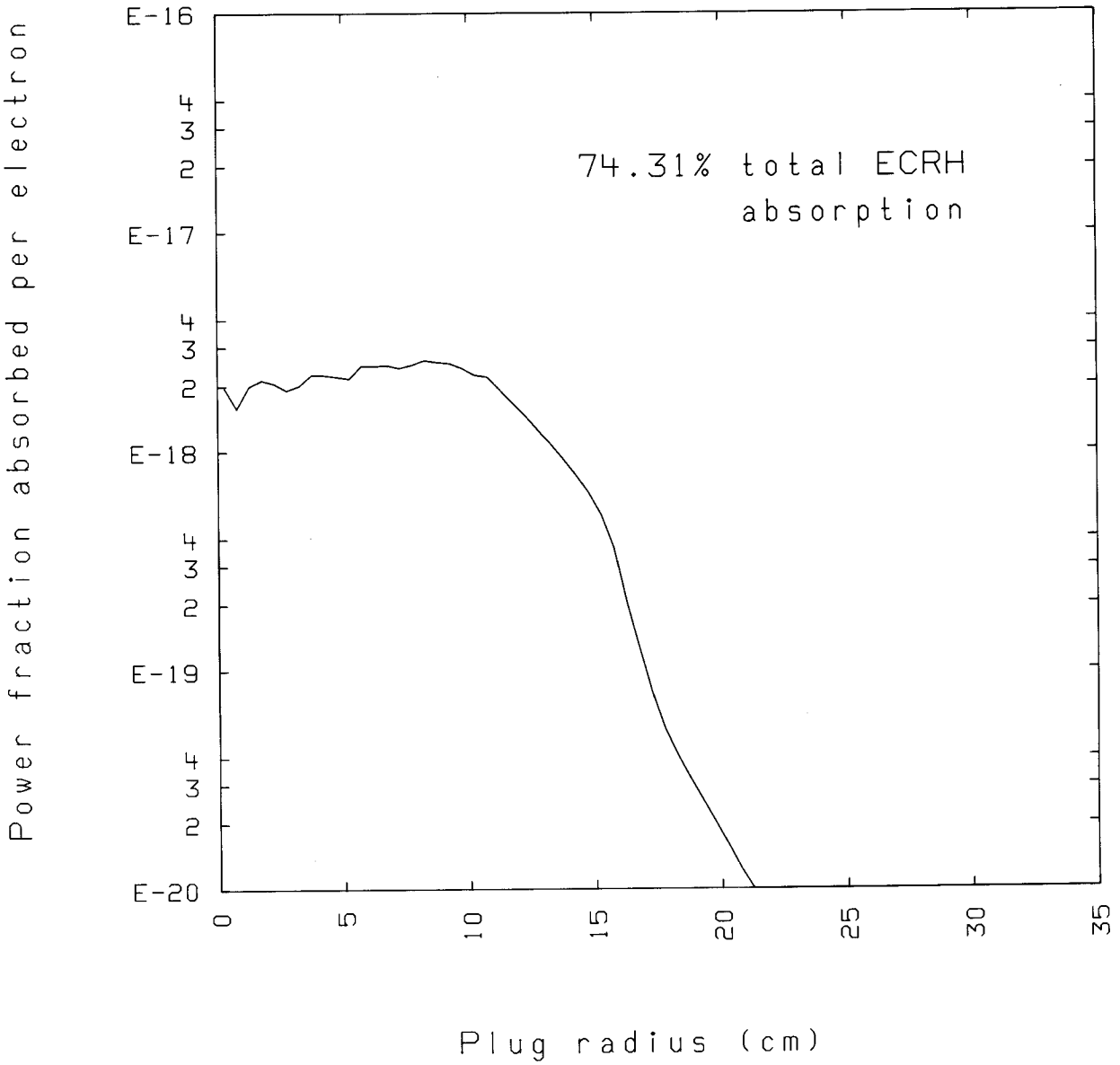

Fig. 9. The fraction of ECRH power absorbed per electron as a function of plug radius using 26 rays, launched as in Fig. 8, to model the plug electron heating in TASKA.

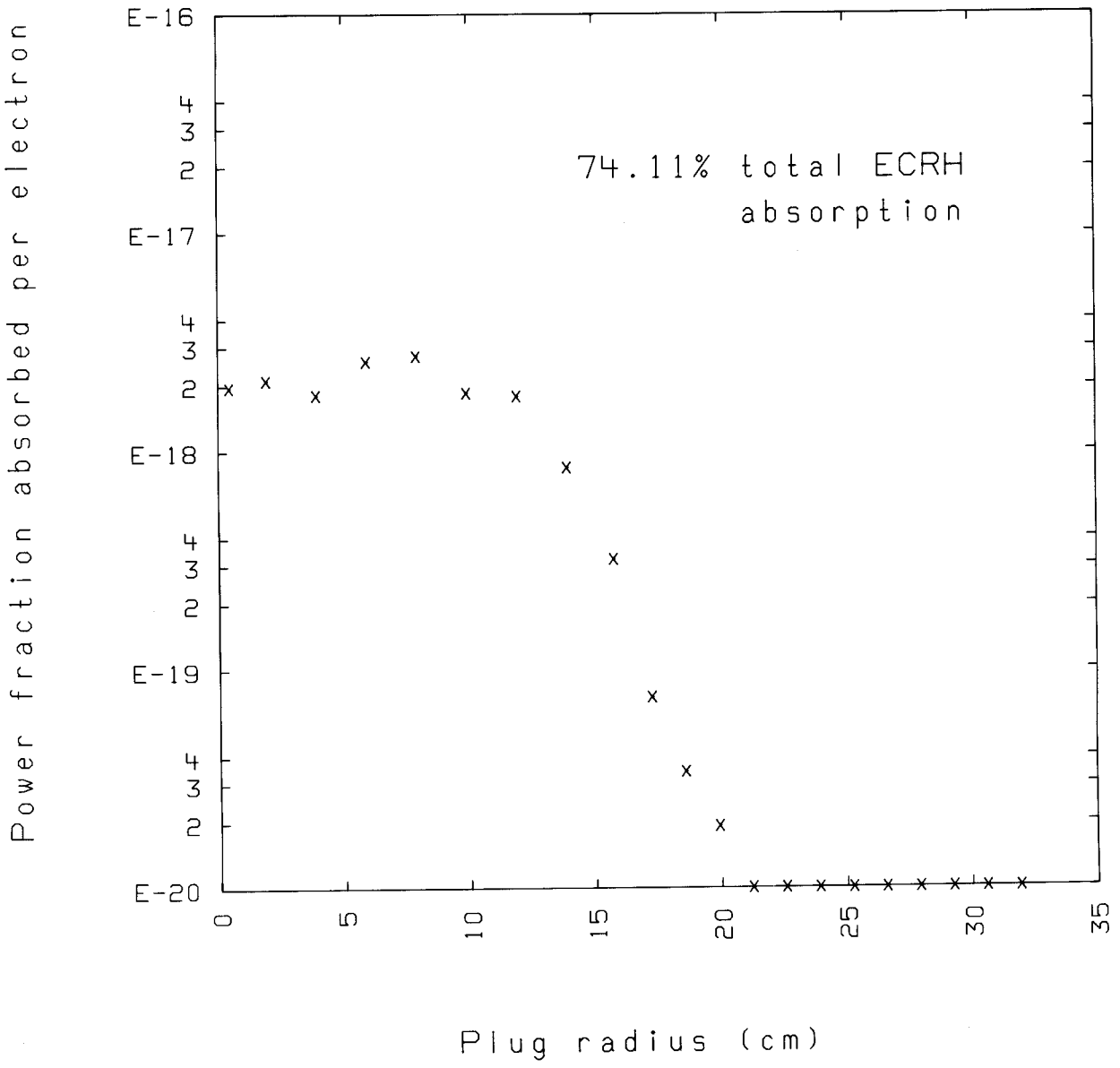

Fig. 10. The fraction of ECRH power absorbed per electron in each radial transport zone using 6 rays, launched as in Fig. 8, to model the plug electron heating in TASKA.

trajectories for each of the multiple rays need not be calculated since for the ordinary mode heating in the TASKA geometry the rays are not bent in the xz plane, but remain straight (see Fig. 6). For a set of rays launched as in Fig. 8 representing strips of power, all will have similar x,z components of their trajectories although there will be substantial bending in the y component. The single ray tracing calculation performed is for the ray launched from the top of the ECRH spot, which is the ray most strongly bent in the y direction. We know a priori that a ray launched at the plasma axis will be unbent in y, remaining in the y = 0 plane throughout its plasma transit, because of the symmetry in y along its trajectory. From this knowledge trajectory points for any number of artificial rays may be constructed by using the x,z coordinates of points along the outer ray, and by using a value for the y coordinate on the i^{th} artificial ray given by

$$y_i(z) = y_{out}(z) \left[\frac{y_i}{y_{out}}\right]_{launch} . \qquad (13)$$

This approximates the various degrees of bending in y for these rays (see Fig. 11).

The plasma absorptivity must be evaluated for each of the artificial rays we have constructed in order that the spatial power deposition may be determined. To do this, at each fixed x,z point we calculate the absorptivity along the outer ray trace, at $y = y_{out}$, along the axis-centered ray, at y = 0.0, and along an intermediate constructed ray at $y = y_{int}$. These 3 points allow a polynomial fit to be made which approximates the absorptivity on the artificial rays:

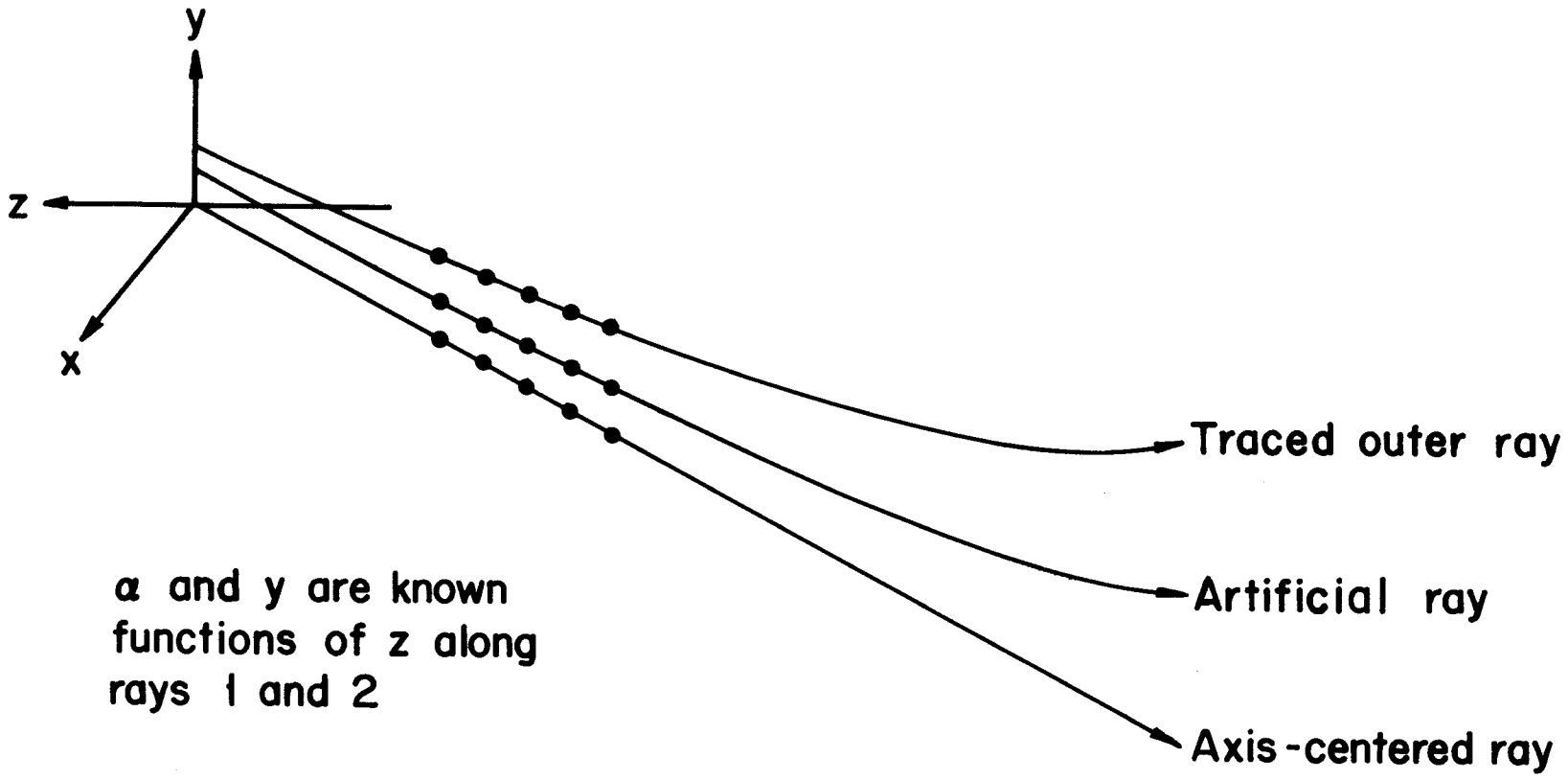

FIGURE 11: CONSTRUCTION OF AN ARTIFICIAL RAY TRAJECTORY IN THE PLANE OF 2 KNOWN RAY TRAJECTORIES.

$$\alpha(y) = a + by^2 \qquad 0 \leq y \leq y_{int}$$

$$\alpha(y) = c + dy \qquad y_{int} \leq y \leq y_{out} \cdot \tag{14}$$

We note that symmetry about y = 0 has been used again and that the form of Eqs. (14) ensure $\alpha(y) > 0$. This is necessary since the absorptivity will often vary by many orders of magnitude from the on-axis to the outer ray, and the use of higher order polynomials will produce oscillations that may then yield negative values for the absorptivity. These lead to large errors in the ray's power deposition due to its exponential nature (Eq. 1) and must be avoided.

With this technique and using Eqs. (13) and (14), any number of artificial rays may be produced from one ray tracing calculation and three evaluations of the plasma absorptivity at each point along the trajectory. We are now free to use as many rays as we wish to avoid pencil beam singularities in the deposition profile and model the ECRH spot. In Fig. 12 we again show the power fraction deposited per electron as a function of plug radius for the same plasma conditions as were used to generate the absorption profiles in Figs. 9 and 10. The ECRH power is now distributed among 50 artificial rays that were generated using the single ray tracing technique. We note that the detailed but time consuming calculation of Fig. 9, where 52 separate ray tracing calculations were performed, is almost identically reproduced. Because of its speed and accuracy, this multiple artificial ray construction will be used to generate the power deposition profiles for the transport code simulations presented in Section IV of this report.

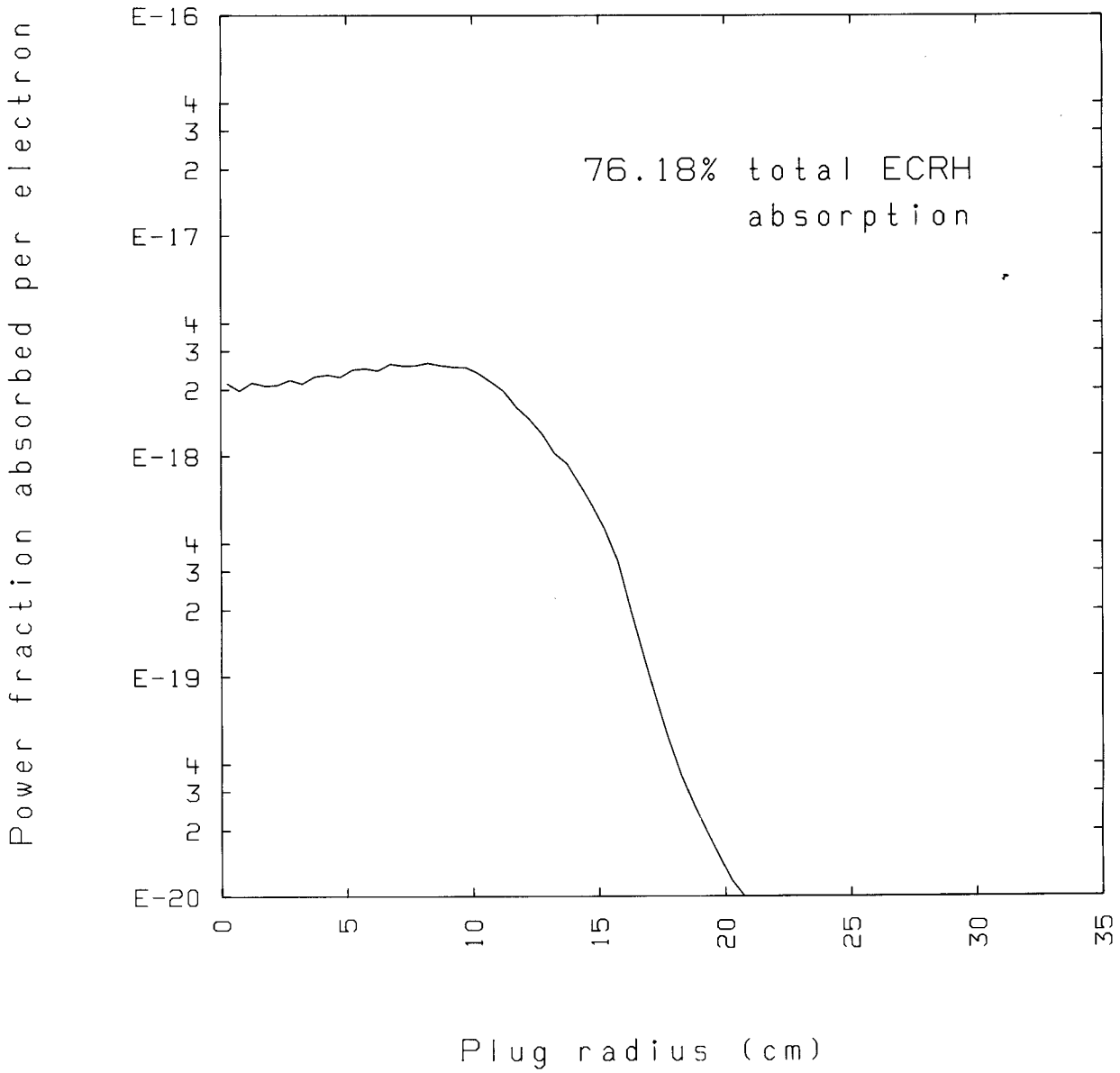

Fig. 12. The fraction of ECRH power absorbed per electron as a function of radius using the artificial ray construction technique to model the plug electron heating in TASKA.

IV. TASKA Startup Simulations with Self-Consistent ECRH Absorption

TASKA is a tandem mirror test facility designed by the University of Wisconsin Fusion Engineering Program and Fusion Power Associates, in association with the Kernforschungszentrum Karlsruhe, FRG. It employs an inboard thermal barrier cell, isolating the central cell electrons from those of the plug, which is created in a minimum-B end cell. The plug electrons are maintained at a higher temperature than those of the central cell by applying ECRH at the fundamental frequency to the 2 Tesla point on the barrier side of the plug magnetic field. The axial magnetic field and resulting axial potential are shown schematically in Fig. 4, while the relevant machine parameters are given in Table 1.

We have added the Audenaerde ray tracing-absorption calculation as a subroutine to the TAMBAR[9] tandem mirror transport code, employing the linkage mechanism described in Section II and modeling the finite spot size of the ECRH system on the plasma using the multiple artificial ray technique based on a single ray tracing calculation as described in Section III. A Boltzmann relation is assumed for the axial density variation on a flux surface, so that as in Eq. (7)

$$n(x,y,z) = n_p(r)e^{-f(z)((\phi_b+\phi_c)/T_{ep})} \tag{15}$$

where ϕ_b is the barrier potential dip, ϕ_c is the plug confining potential, and where f(z) is a shape function taken from Li[11] that describes the axial variation of the TASKA plasma potential between the barrier minimum and the plug maximum. We have also added finite beta (β = plasma pressure/volume magnetic field pressure) corrections to the plug vacuum magnetic field, which

Table 1. TASKA Machine Parameters

Dimensions	
Central cell length	19.2 m
Barrier length	14.5 m
Plug length	5.1 m
Central cell plasma radius	0.32 m
Plug plasma radius	0.28 m
Magnetic Fields (On-Axis)	
Central cell	2.7 T
Barrier maximum	20 T
Barrier minimum	0.8 T
Plug maximum	6.25 T
Plug minimum	4 T
Heating	
Plug neutral beams	2.7 MW, 250 keV, injected 60°
Barrier pump neutral beams	49.7 MW, 50 keV, injected 25°
	6.6 MW, 76 keV, injected 20°
Plug ECRH	7.45 MW @ 56 GHz
Central cell ICRH	40 MW @ 21 MHz
Equilibrium Plasma Parameters (On-Axis)	
Central cell density, n_c	1.9×10^{14} cm^{-3}
Barrier minimum density, n_b	6.8×10^{12} cm^{-3}
Plug density, n_p	6.3×10^{13} cm^{-3}
Central cell ion temperature, T_{ic}	30 keV
Central cell electron temperature, T_{ec}	11.5 keV
Plug ion energy, $\bar{E}_p$	388 keV
Plug electron temperature, T_{ep}	59 keV
Floating potential, ϕ_e	66 kV
Barrier potential dip, ϕ_b	38 kV
Plug potential increase, ϕ_c	43 kV
Central cell beta, β_c	0.50
Plug beta, β_p	0.64
Fusion power	86 MW
Q	0.74
Central cell wall loading	1.52 MW/m^2

impact both the plug ion confinement via the enhanced mirror ratio, and the flux mapping mechanism of Section II.

We have used this modified transport code to study the proposed startup scenario for TASKA, and in particular to study the effects of local ECRH power absorption on the plasma evolution. The central cell and the end plugs are initially filled with a stream gun plasma, which is then built up to its equilibrium values using the combinations of neutral beams given in Table 2. The plug density is built up before that of the central cell so that the β-averaged macrostability of the machine is assured, and so that with the confining ϕ_i produced in the plugs, the central cell plasma may be built up using only the steady state beams. Since the trapping fraction for the 250 keV plug neutral beams on the stream gun plasma would be too small to produce plasma buildup, 500 amperes of 15 keV neutral beams are used initially to maintain the plug plasma density while also increasing the mean ion energy, $\bar{E}_p$, to 15 keV. At 15 ms the 15 keV beams may be turned off and the 250 keV beams are applied at their steady state currents.

The central cell beams are located in the barrier cells of TASKA, and serve the dual purpose of pumping out the barrier cell so as to produce the potential dip ϕ_b, while at the same time fueling the central cell. The pump beams are oriented so that the ions produced from charge exchange and impact ionization appear as sources for the central cell plasma. These central cell beams are brought to their steady state currents at the 15 ms point of the simulation, so that the central cell density continues to increase to its equilibrium value throughout the simulation.

The transport code calculates the barrier potential dip from the expression[12]

Table 2. TASKA Startup Scenario

Stream Gun Plasma

Central cell density (r = 0)	1.0×10^{13} cm^{-3}
Plug density (r = 0)	2.0×10^{13} cm^{-3}
Central cell temperature (ion, electron)	100 eV
Plug temperature (ion, electron)	100 eV

Neutral Beam Injection

	0.5 ms	5-15 ms	> 15 ms
Central cell			
46 keV	586 Amp	586 Amp	1173 Amp
Plug			
15 keV @ 90°	500 Amp	261 Amp	0
250 keV @ 70°	0	5.4 Amp	10.8 Amp

$$e^{-\phi_b/T_{ec}} = \frac{g_b}{R_b}\sqrt{\frac{T_{ic}}{\pi\phi_b + T_{ic}}} \tag{16}$$

where R_b is the barrier mirror and the pumpout parameter, g_b is equal to the ratio of the total density in the barrier (barrier trapped particles and central cell streaming plasma) to the streaming density. This factor models the effectiveness of barrier pumping and must be supplied to the transport code. We have used a radially varying expression,

$$g_b = 2.0 + 2.5\left(\frac{r}{30\ cm}\right) \tag{17}$$

where r is the flux surface's radius in the plug, so that the spatial variation of the barrier pump beam may be simulated.

From a startup calculation using the neutral beam scenario of Table 2, but with no ECRH power added to the plug electrons, we plot at 40, 80 and 120 ms into the simulation the radial profiles of the plug electron temperature, the plug mean ion energy, the plug density and the central confining potential ϕ_c in Figs. 13, 14, 15, and 16, respectively. The 40 ms plug electron temperature profile illustrates the extent to which plug electrons may be heated by hot ion drag in a scenario where the plug plasma is built up first. A low initial central cell density minimizes the power plug electrons lose to the colder central cell electrons that are streaming into the plug. The heating of plug electrons by drag to temperatures above 5 keV is significant since ECRH power absorption for the ordinary mode is very small below these temperatures. This neutral beam heating removes the need for an additional ECRH system using the extraordinary mode, whose absorptivity is greater at low

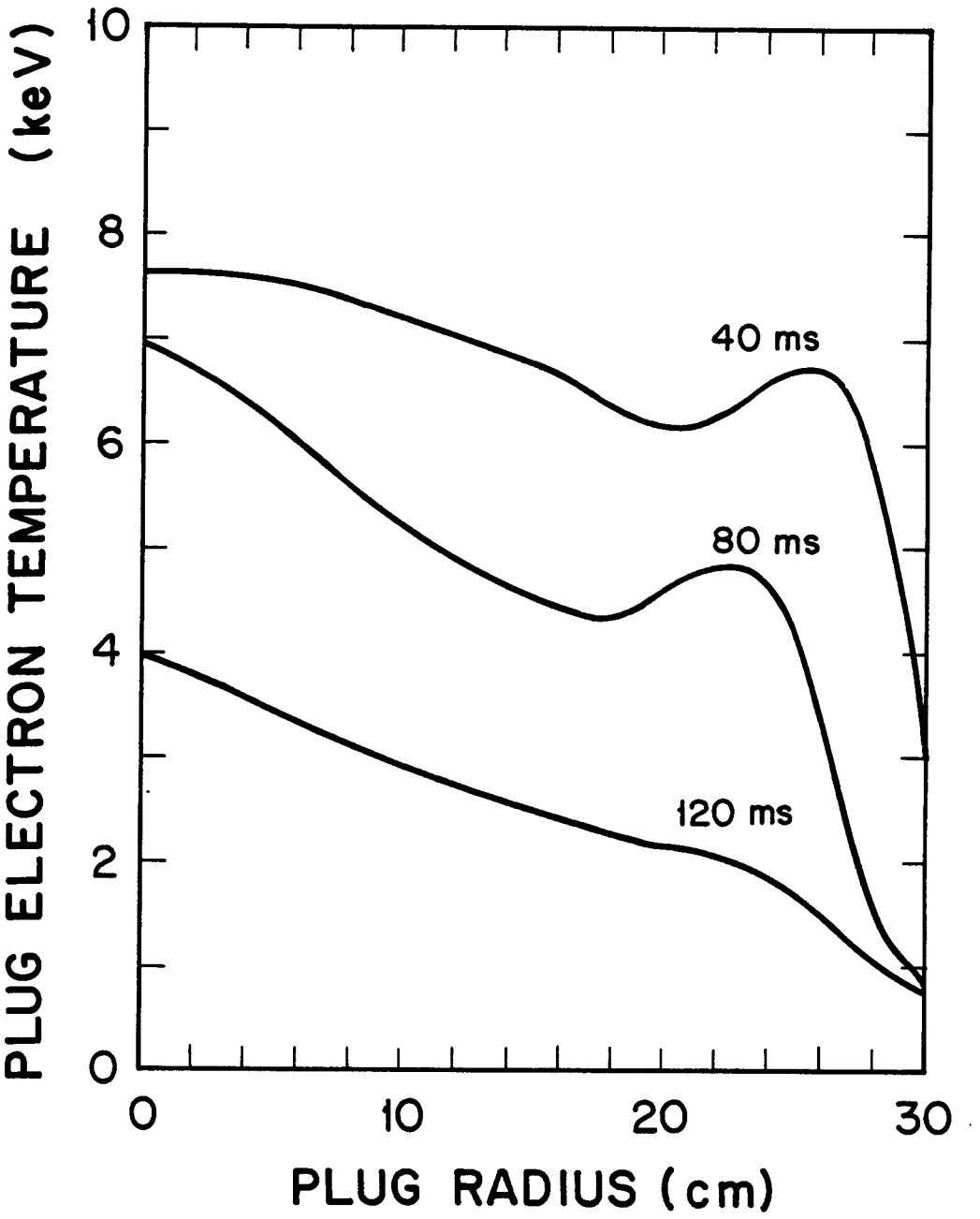

Fig. 13. Radial plots of the plug electron temperature for a startup simulation without ECRH.

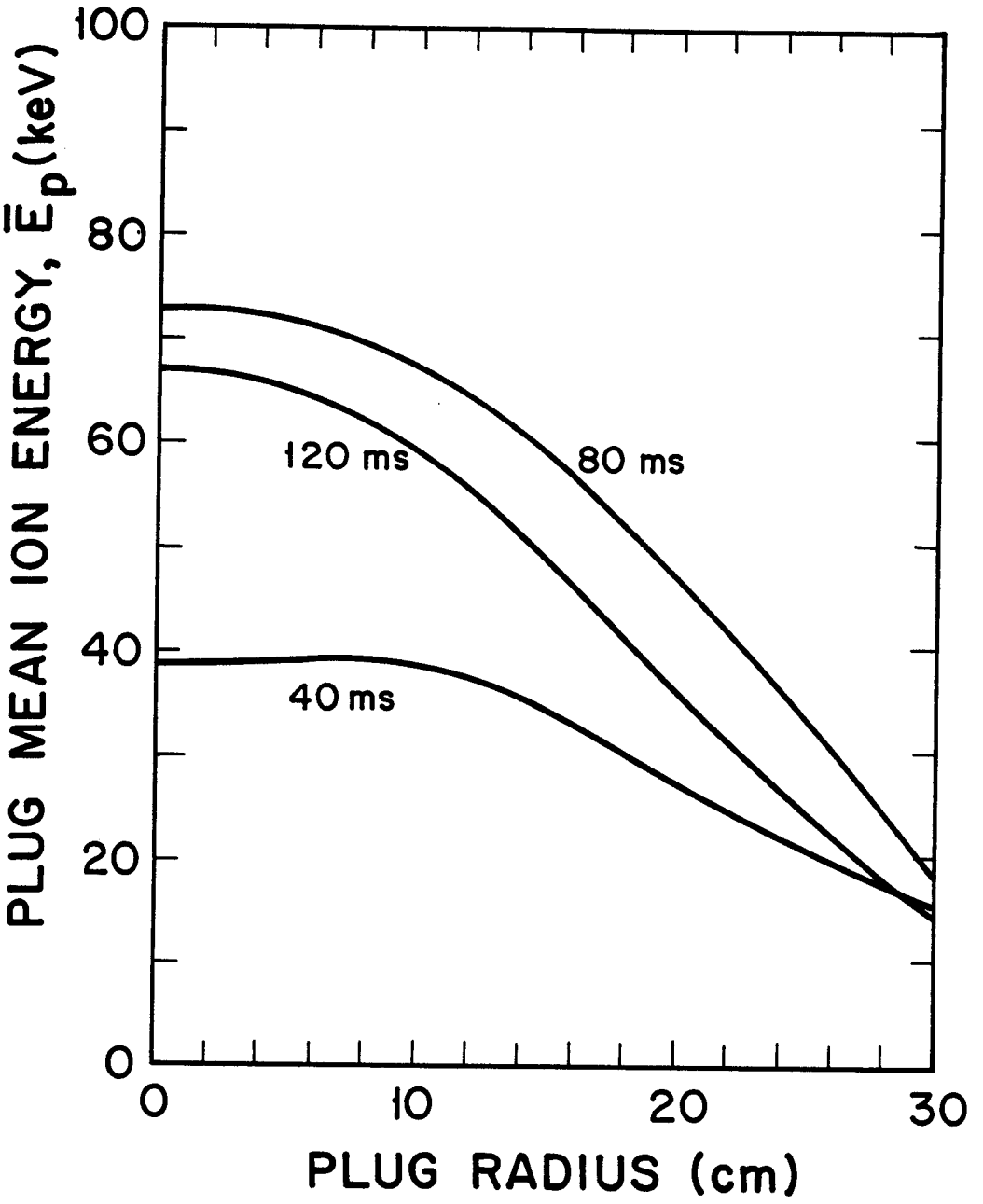

Fig. 14. Radial plots of the mean plug ion energy for a startup simulation without ECRH.

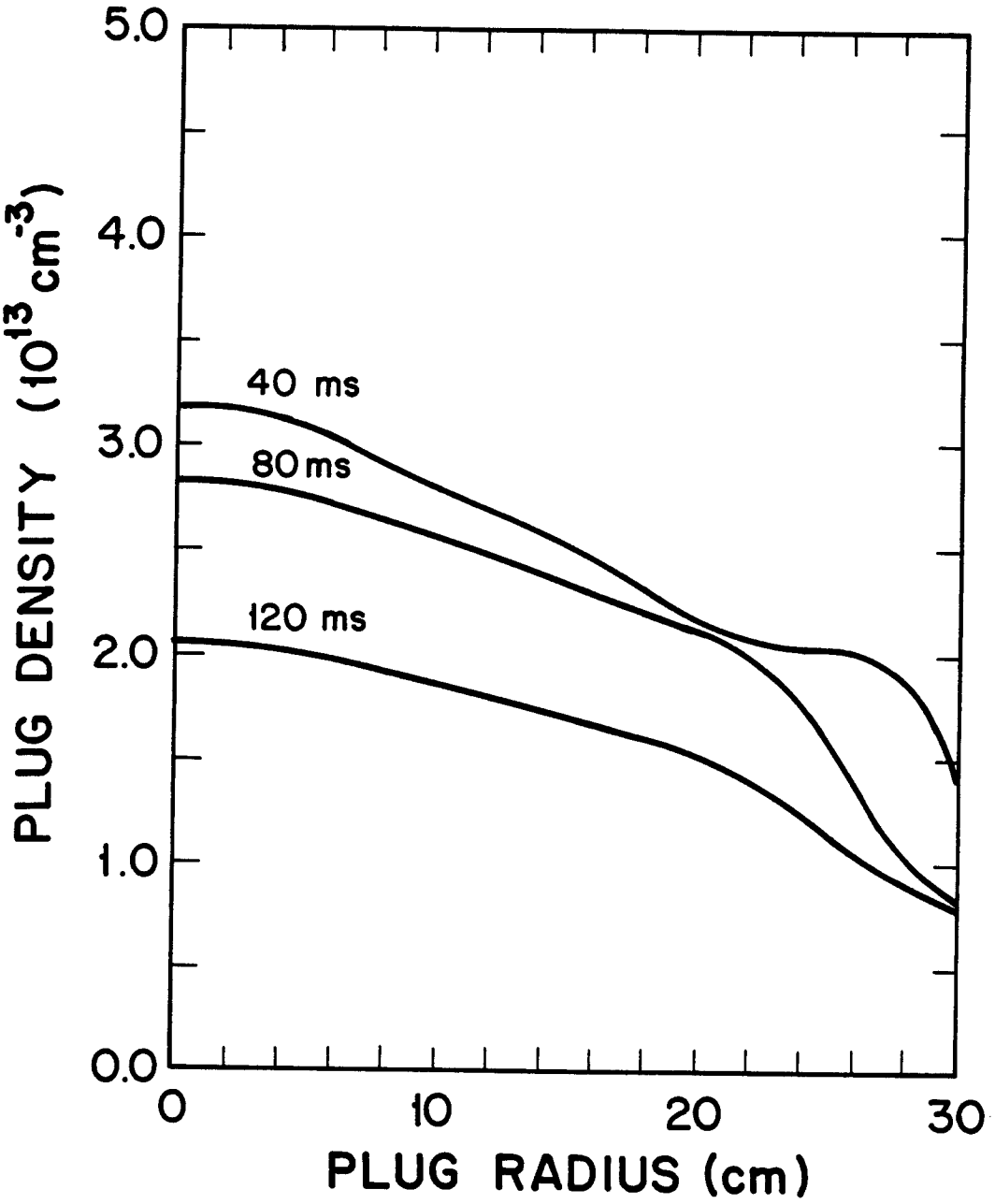

Fig. 15. Radial plots of the plug density for a startup simulation without ECRH.

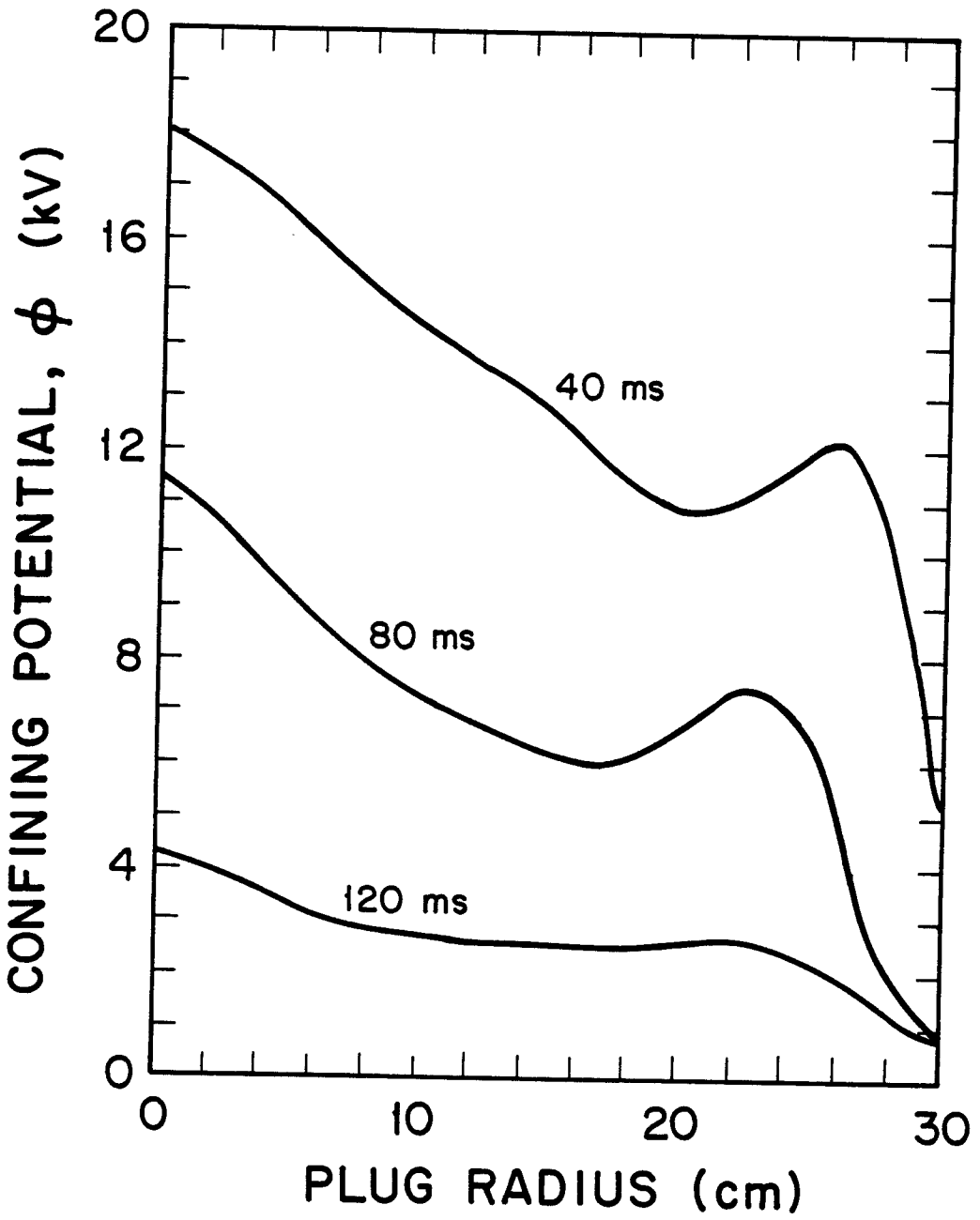

Fig. 16. Radial plots of the plug confining potential for a startup simulation without ECRH.

electron temperatures, and which would normally be required to raise the electron temperatures from their initial values.

At times greater than 40 ms into this scenario without ECRH, the plug electron temperature falls as a result of greater energy loss to the colder streaming central cell electrons, whose density is increasing toward its equilibrium value. The need for auxiliary plug electron heating to maintain high electron temperatures is apparent as the falling temperatures directly restrict the plasma evolution in two ways. The plug electrons, now unable to rise significantly above the central cell electron temperature, drag on the plug ions preventing their mean energy from continuing its rise, as shown in Fig. 14. The large electron drag and low ion energy also make the plug ion confinement time much lower than desired and, as Fig. 15 illustrates, the plug density decreases as a result. Secondly, the small temperature difference between the central cell and plug electrons means that the plug potential rise that confines the central cell ions, given by[13]

$$e(\phi_b + \phi_c) \cong T_{ep} \ln \left[\frac{n_p}{n_b} \left(\frac{T_{ec}}{T_{ep}}\right)^{0.5}\right], \tag{18}$$

will decrease as the central cell density is built up, as is shown in Fig. 16. The low values of ϕ_c mean that there is now very little electrostatic trapping of central cell ions. Figures 13-16 illustrate that additional plug electron heating, ECRH, is required during this startup scenario to keep the electron temperature sufficiently high.

Having shown the importance of auxiliary heating to maintain high plug electron temperatures against increasing central cell energy losses, we now illustrate a danger of supplying ECRH power at a rate much greater than that

at which power is lost by other mechanisms. The dominant energy loss processes for plug electrons are rethermalization on the central cell streaming plasma and the loss of energetic electrons from the mirror trap. Both of these loss rates are proportional to the electron collision frequency, which goes as $T_e^{-3/2}$. Thus, as ECRH heats the electrons to higher temperatures, their energy loss rate decreases since it is dominated by rethermalization and end-loss. This will result in further electron temperature increases, and since the plasma absorptivity generally increases with greater temperatures, the ECRH power deposition will then also increase. In this way a feedback mechanism is set up between the rising electron temperature on the one hand, and lower collisional energy losses with greater ECRH heating on the other.

In the end-loss dominated mirror cell, this temperature rise may furthermore be spatially localized since radial energy transport occurs on a slower time scale than rethermalization and end-loss, and therefore cannot diffuse a local temperature spike produced by these two processes. We have included in the transport code bremsstrahlung energy losses given by the expression[14]

$$P_{Br} = 1.57 \times 10^{-32}\ n^2 T_e \qquad [\text{watts/cm}^3]$$

where the density is in units of cm^{-3} and the electron temperature is in eV, as well as included synchrotron radiation energy loss and transport by adding the Cytran[15] calculation as a subroutine. However, at the electron temperatures simulated here these radiation losses are small and the dominant energy loss processes remain end-loss and rethermalization.

In Fig. 17 we show the time evolution of the radial plug electron temperature for a simulation using the neutral beam scenario of Table 2 and launch-

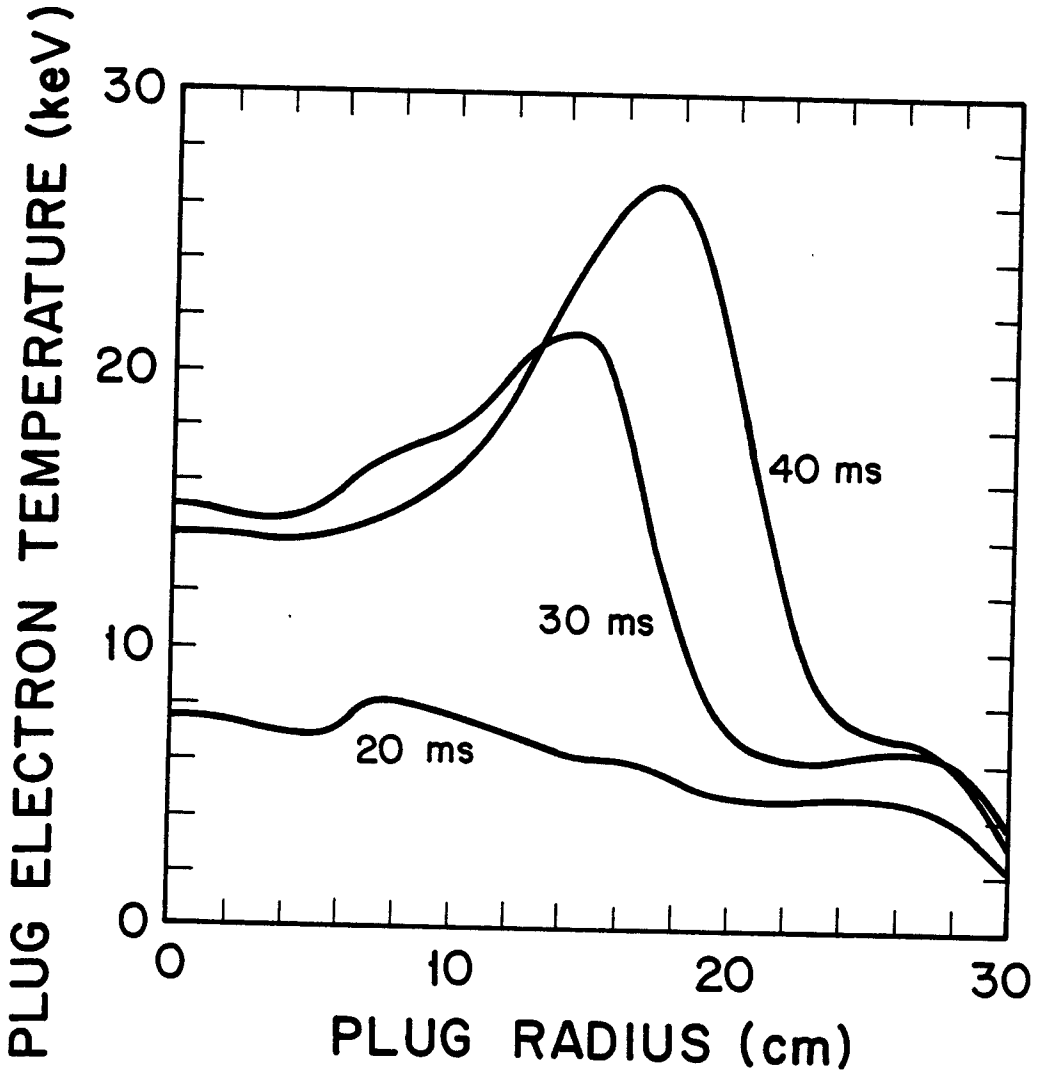

Fig. 17. Radial plots of the plug electron temperature for a startup simulation with 250 kW of ECRH.

ing 250 kW of ECRH power into the plug starting at 15 ms. For this calculation we have used the launch point specified in the TASKA design. The radial profiles for the ECRH power deposition were calculated by calls to the ray tracing subroutine every 35 time steps, or about every 5 ms. The results of this self-consistent heating calculation in Fig. 17 show first of all the rapid rise in the electron temperature produced by this power input. In Fig. 18 the central cell confining potentials that these temperatures produce in the plug is shown, and in Fig. 19 the radial profiles of the plug density at the same times into the simulation are shown. There is a strong correlation between the rise and the shape of the electron temperature and confining potential profiles, as is expected by Eq. (18). We also wish to point out that the large plug potentials produced by the strong electron heating of this scenario impact ion confinement in the plug. These plasma potentials eject ions from the mirror cell, since the mean plug ion energy is still low early in the startup scenario. This effect is shown in Fig. 19.

The most noticeable feature of the electron temperature evolution in Fig. 17 is the local temperature spike at 40 ms that results from the feedback mechanism described above. In Fig. 21 we show the x,z trajectory for a ray at the 40 ms point of the simulation, and in Figs. 20 and 22 the radial ECRH power deposition profiles for the 20 and 40 ms points, respectively. The radial power deposition profile at 20 ms is fairly flat at small radii, and the electron heating caused would not by itself create such a large temperature spike. However, a local imbalance at 15 cm between the electron energy loss rate and the ECRH heating rate results in a temperature rise there. Through decreasing energy loss rates and increasing local ECRH absorption, this is soon transformed into the large temperature spike in Fig. 17 at 40 ms.

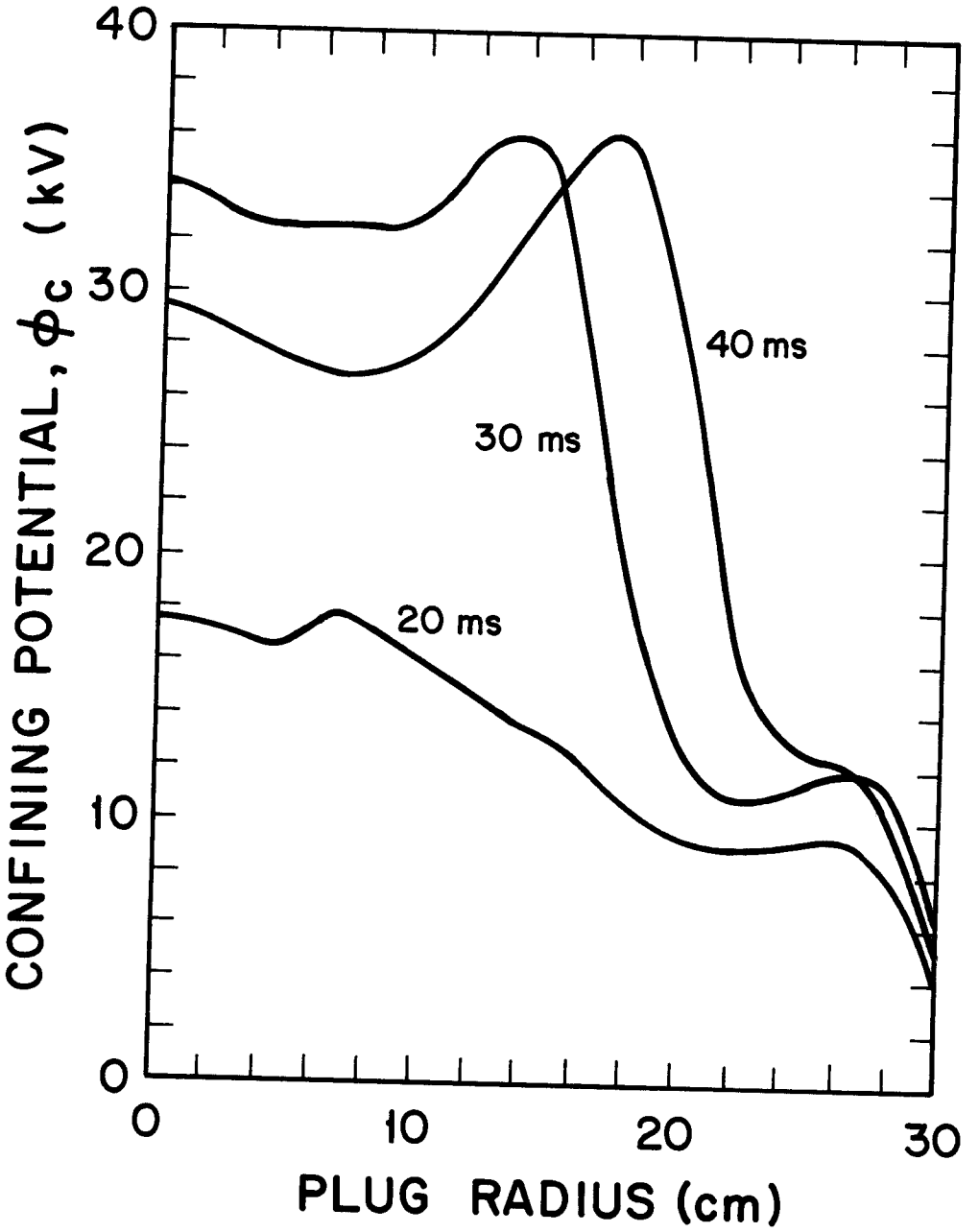

Fig. 18. Radial plots of the plug confining potential for a startup simulation with 250 kW of ECRH.

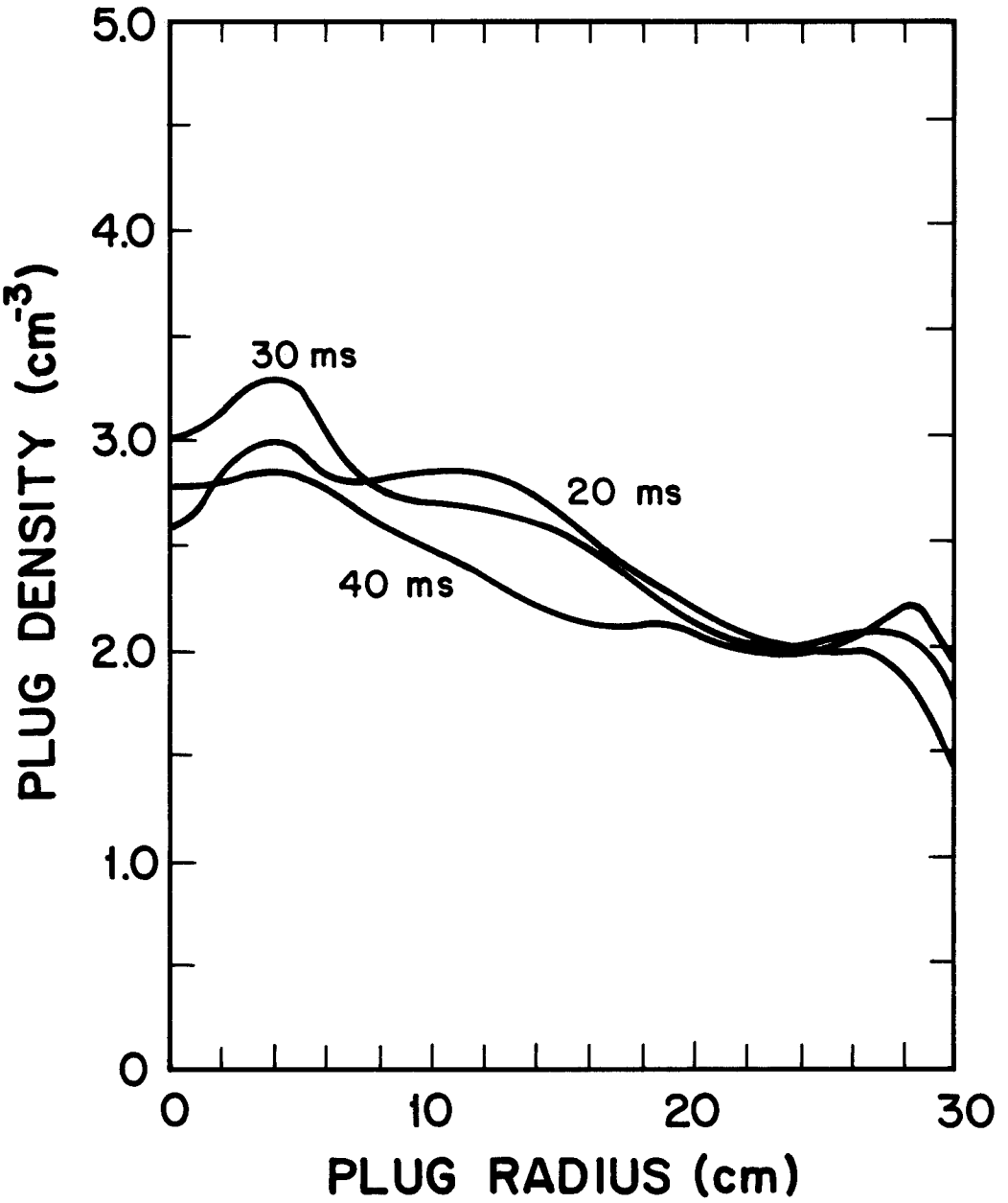

Fig. 19. Radial plots of the plug density for a startup simulation with 250 kW of ECRH.

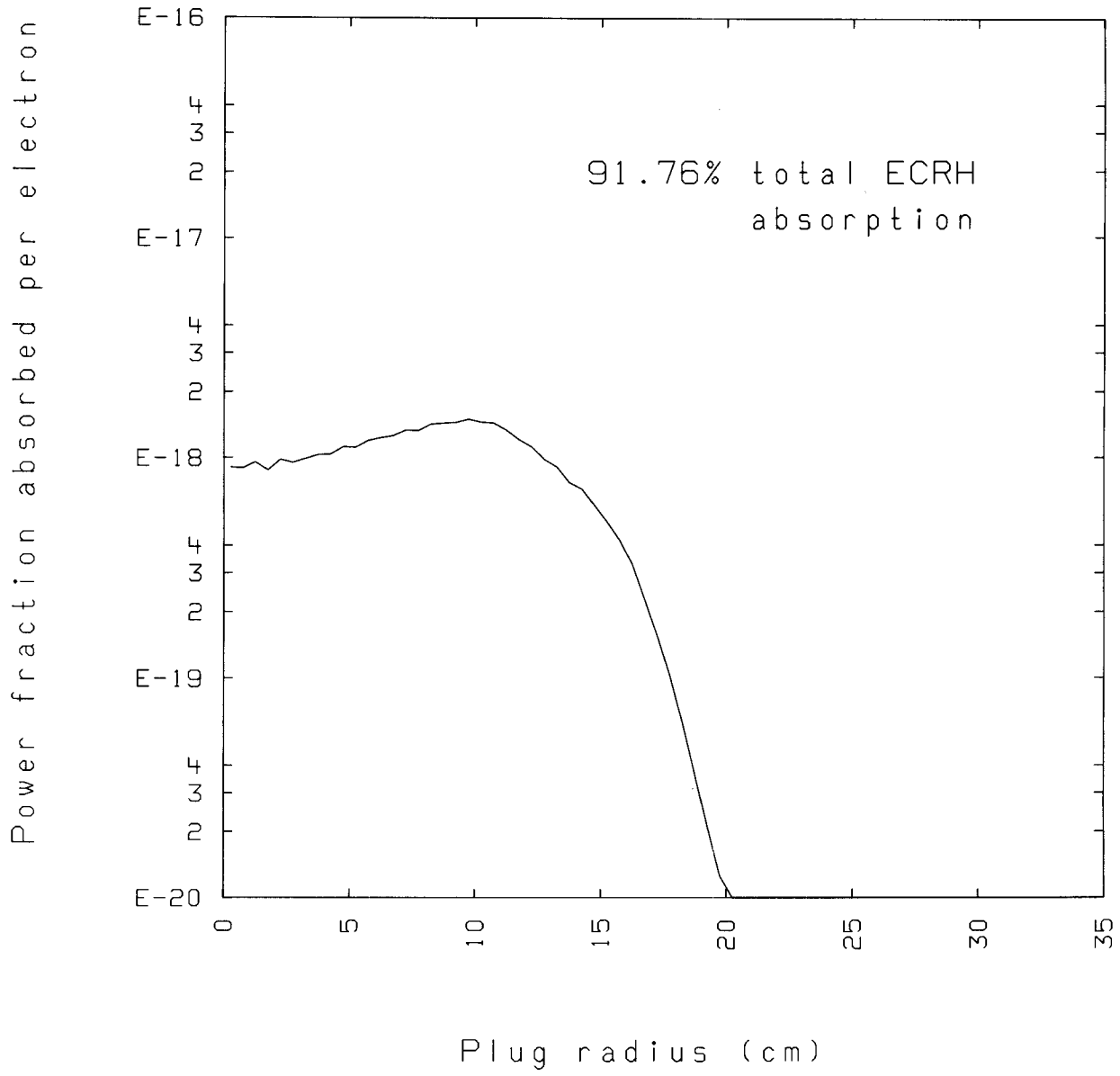

Fig. 20. The fraction of ECRH power absorbed per electron as a function of radius at the 20 ms point of the simulation described in Figs. 17, 18 and 19.

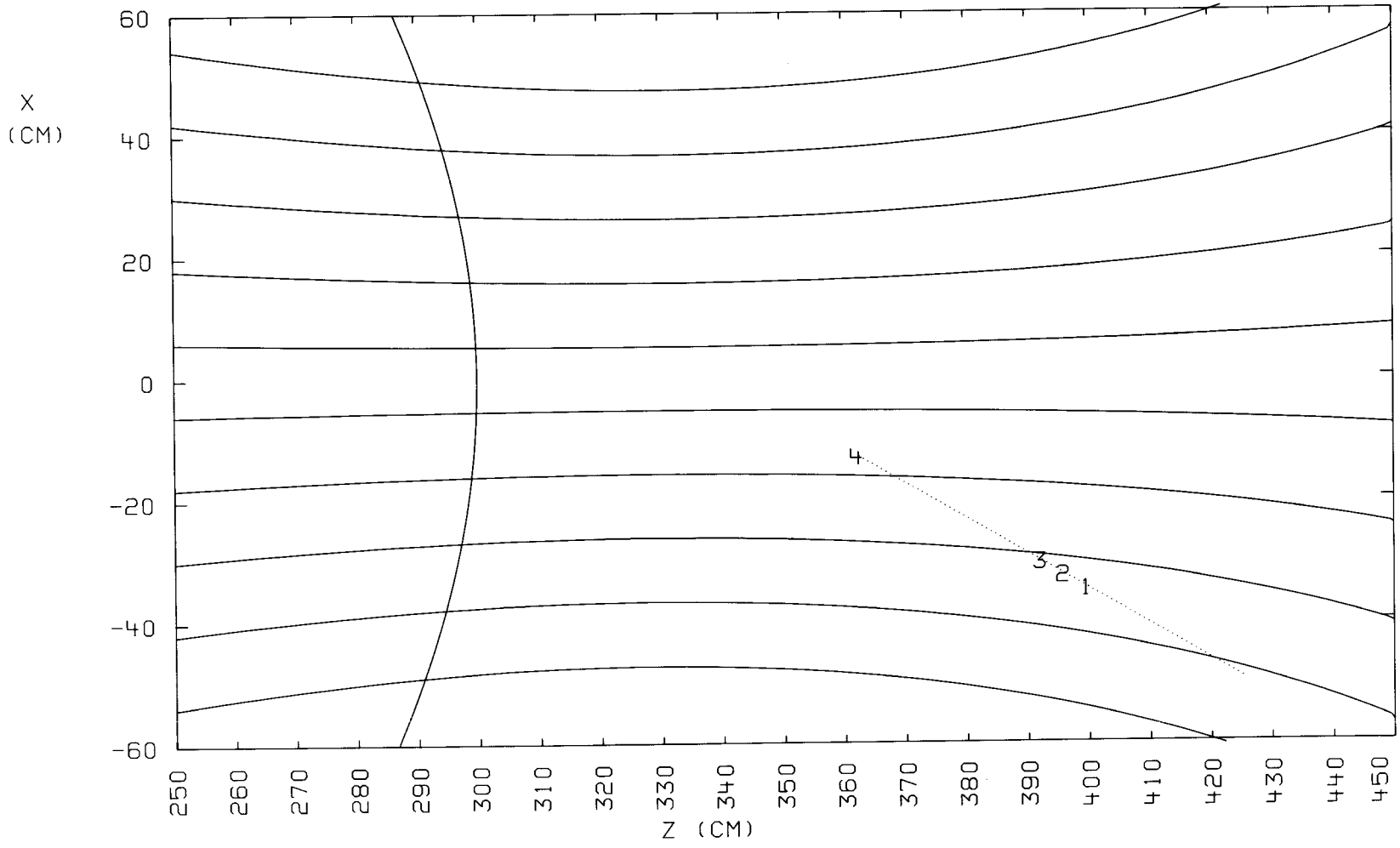

Fig. 21. The ray trajectory for the TASKA design launch at the 40 ms point of the simulation described in Figs. 17, 18 and 19. The ECRH power deposition is denoted by: 1 = 25%, 2 = 50%, 3 = 75%, and 4 = 99.9% power absorbed.

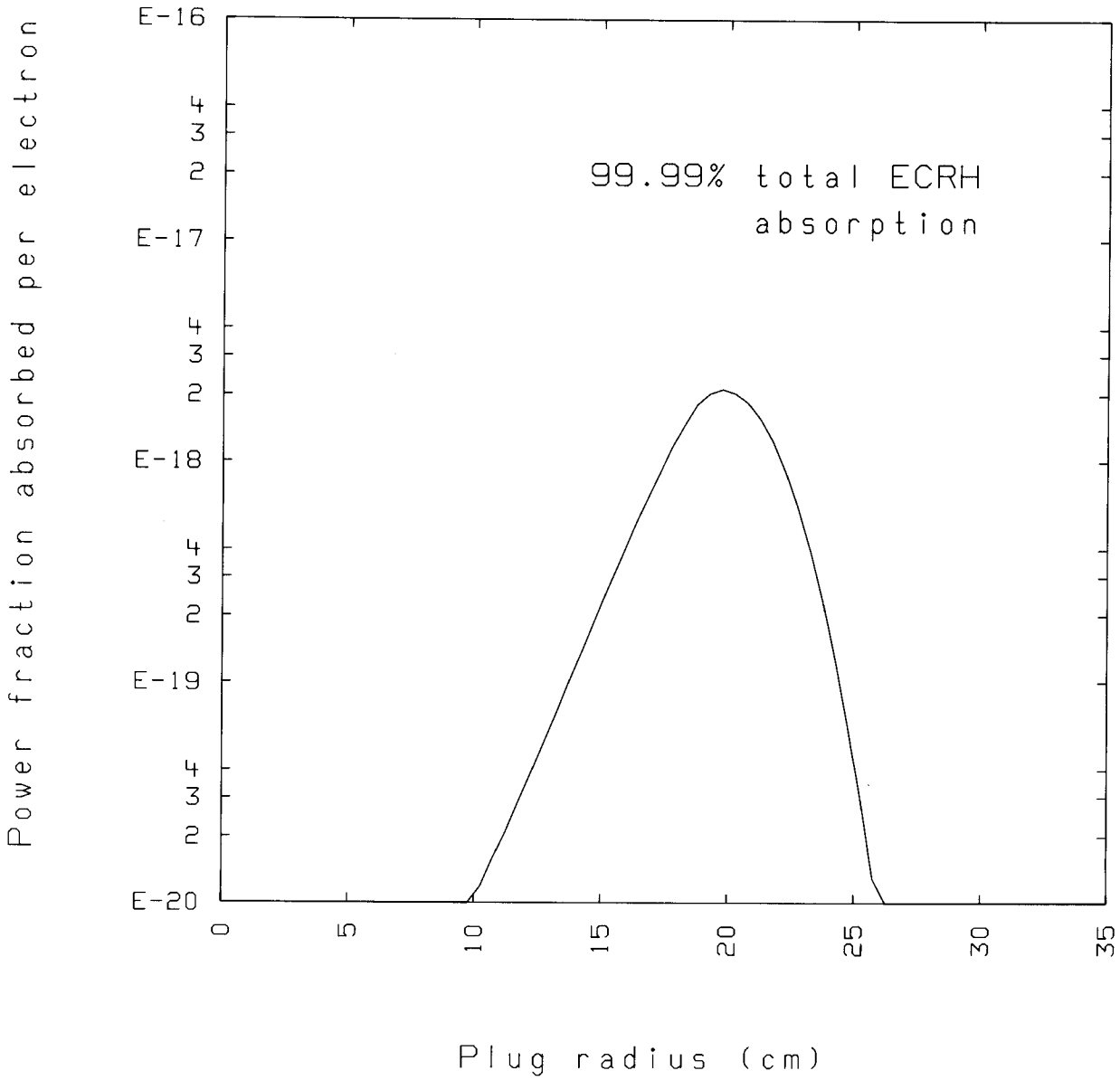

Fig. 22. The fraction of ECRH power absorbed per electron as a function of radius at the 40 ms point of the simulation described in Figs. 17, 18 and 19.

That such a large change can occur in the temperature profile in such a short amount of time is evidence of the strength of the feedback mechanism at high power levels. As Figs. 21 and 22 show, the entire system's ECRH power is now deposited just beneath the plasma surface. Because the power deposited along a ray, given by Eq. (1), has an exponential drop off along the ray trajectory, even less severe temperature peaks near the plasma edge will shield the inner plasma from the ECRH, decreasing the electron heating there. Figure 17 illustrates the falling electron temperatures at small radii while those nearer the edge rise for this extreme example. Obviously, it is desirable that such large radial variations in the electron temperature do not occur.

As these two simulations have shown, the role of ECRH in this startup calculation is to maintain the plug electrons at temperatures sufficiently high so that electron drag does not restrict plug ion evolution, yet at the same time not heat them so high as to result in enhanced plug ion losses from a large plasma potential. To do this the ECRH power input must very nearly balance the plug electron energy loss, which is increasing with time due to larger rethermalization losses on the streaming central cell electrons. This task is complicated by the need to reach this balance in each radial zone since in an end-loss dominated device radial transport is insufficient to smooth large variations in the radial profiles. If at a particular radius the electron heating is too strong and there is a localized temperature rise, a temperature spike will soon result due to decreased energy losses and increased ECRH absorption. This electron temperature spike usually appears off the plasma axis and shields the plasma in the center from the ECRH by its strong absorptivity. We now present a simulation in which this balance has been maintained during the initial 100 ms of the simulation. The same neutral

beam scenario is used as was previously, that of Table 2, and to avoid overheating the electrons, modest ECRH power levels that increase with time were used and are given in Table 3. The launch point was also moved to an axial position where the plasma density is lower, and a sharper launch angle across the plasma was used so that the path length of a ray through a radial transport zone would be shorter. Both of these were done in an effort to reduce the ECRH power deposition in the case of a temperature spike. The heating trajectory used is shown in Fig. 23.

The radial plots of the plug electron temperature, the plug mean ion energy, the plug density, the central cell confining potential produced and the central cell density for this startup simulation at times 40, 80 and 120 ms are shown in Figs. 24-28. The radial ECRH power deposition profiles calculated by our ray tracing subroutine are shown in Figs. 29-31 for the 40, 80 and 120 ms times. By comparing the radial profiles of this scenario to those of the same time in Figs. 13-16 in which no ECRH power was added, it is seen that this startup scenario proceeds nicely until 100 ms into the simulation. The plug electrons are maintained by the injected ECRH power at reasonable temperatures that are spatially without large peaks, the plug ions continue to increase their mean energy free from electron drag, the plug plasma density is maintained, and a confining potential is produced in the plug that creates a significant buildup of central cell plasma. At 120 ms however, a local temperature spike is forming as in the previous scenario. We note again the resulting change in the confining potential's radial profile, the drop in the electron temperature behind the peak, and the change in the radial ECRH power deposition profile at 120 ms to have a maximum at the temperature peak, where previously the profile was uniform.

Table 3. Launched ECRH Power Levels Increasing With Time

Time Into Simulation	ECRH Power
25-50 ms	75 kW
50-75 ms	125 kW
75-100 ms	200 kW
100-125 ms	300 kW

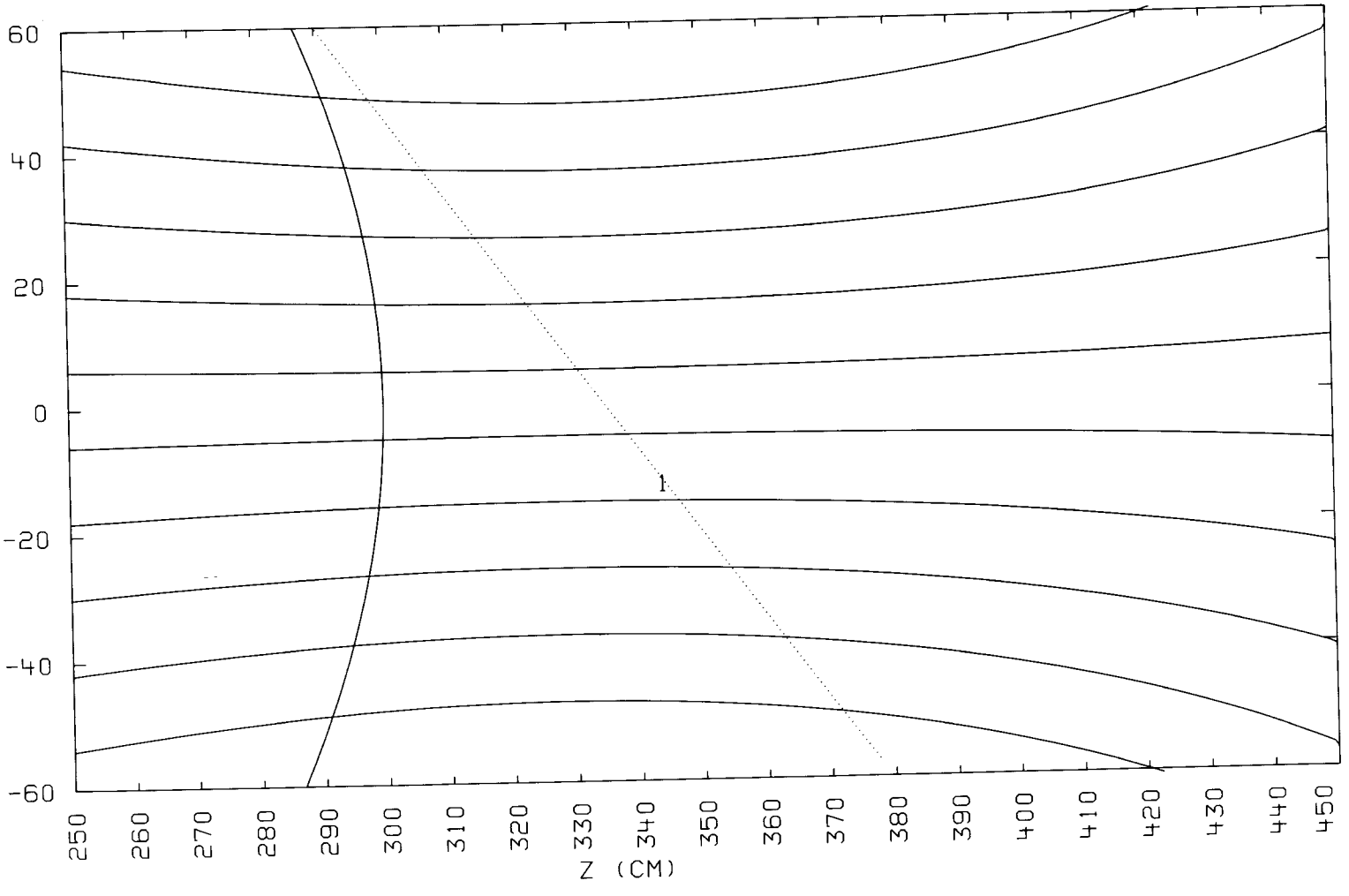

Fig. 23. The ray trajectory for the modified TASKA launch at the 40 ms point of the simulation described in Figs. 24-28. The ECRH power deposition is denoted by: 1 = 25%, 2 = 50%, 3 = 75%, and 4 = 99.9% power absorbed.

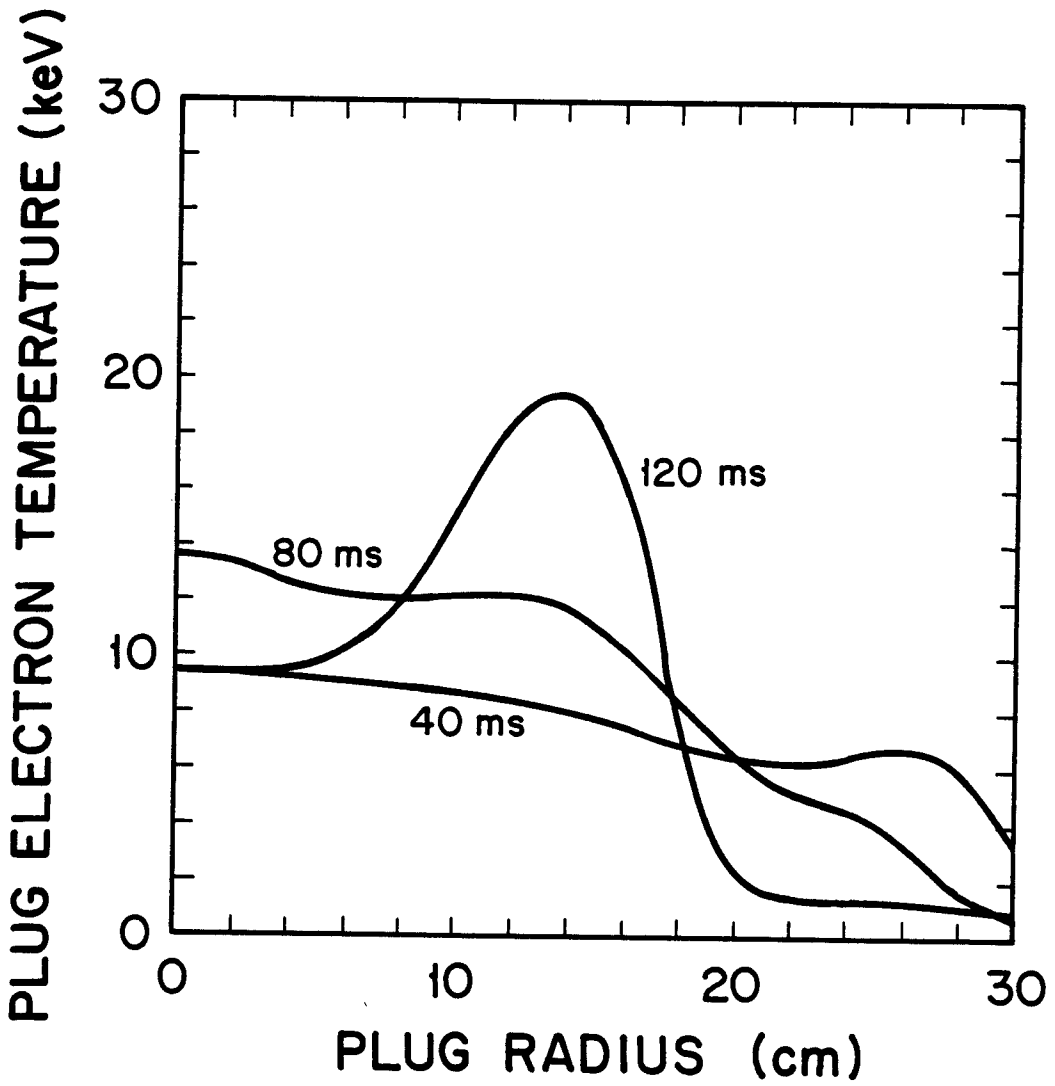

Fig. 24. Radial plots of the plug electron temperature for a startup simulation using the ECRH power levels of Table 3.

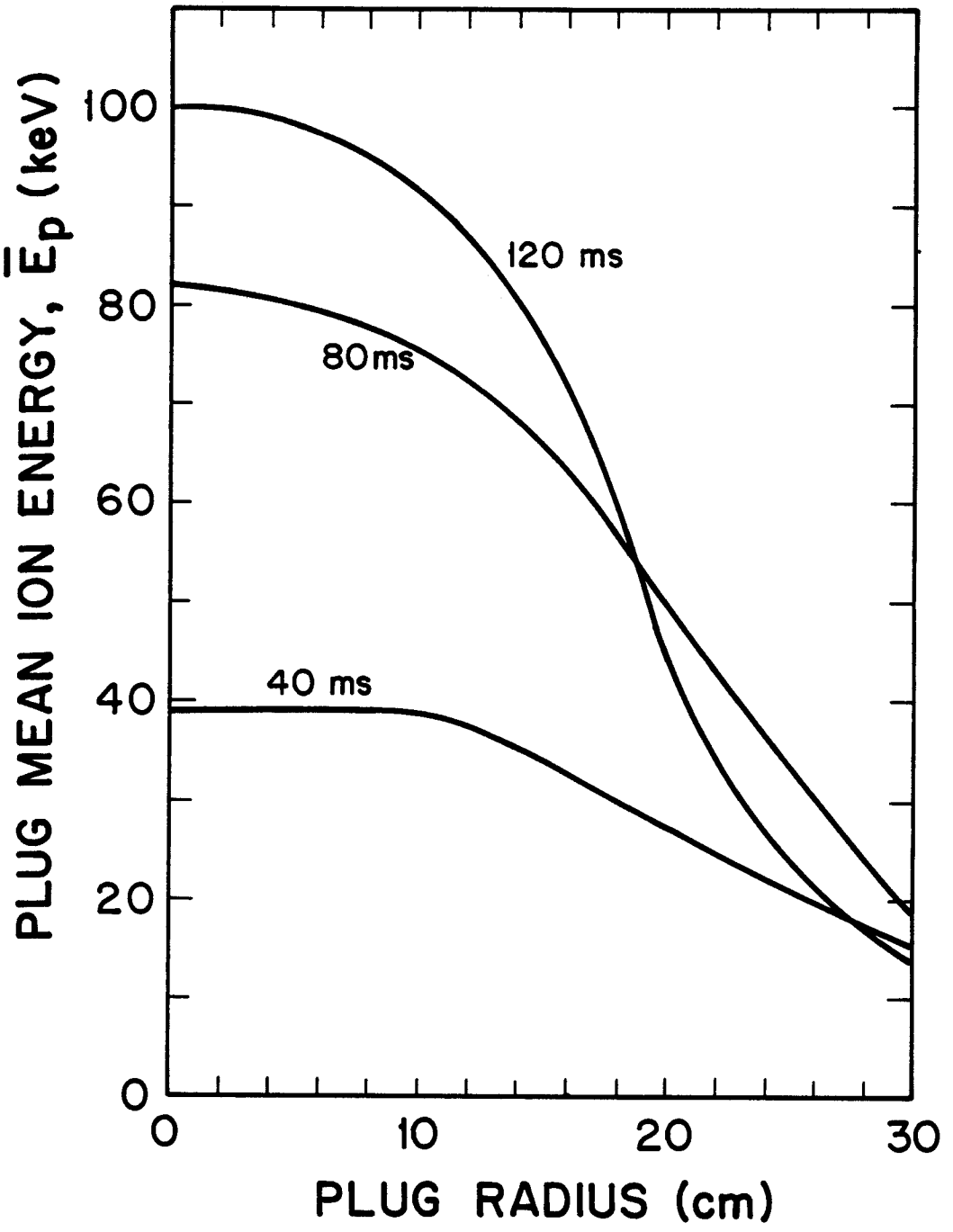

Fig. 25. Radial plots of the plug mean ion energy for a startup simulation using the ECRH power levels of Table 3.

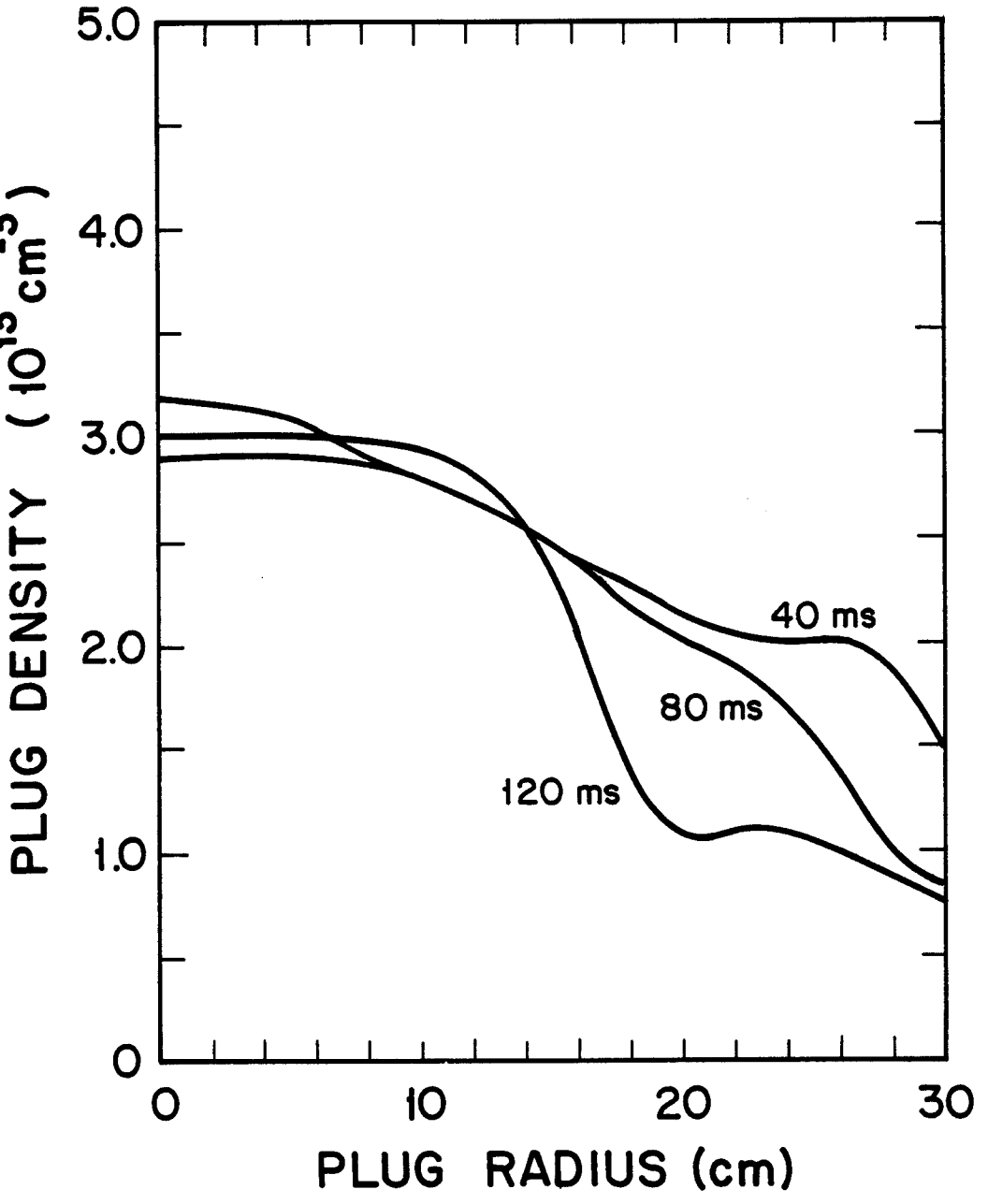

Fig. 26. Radial plots of the plug density for a startup simulation using the ECRH power levels of Table 3.

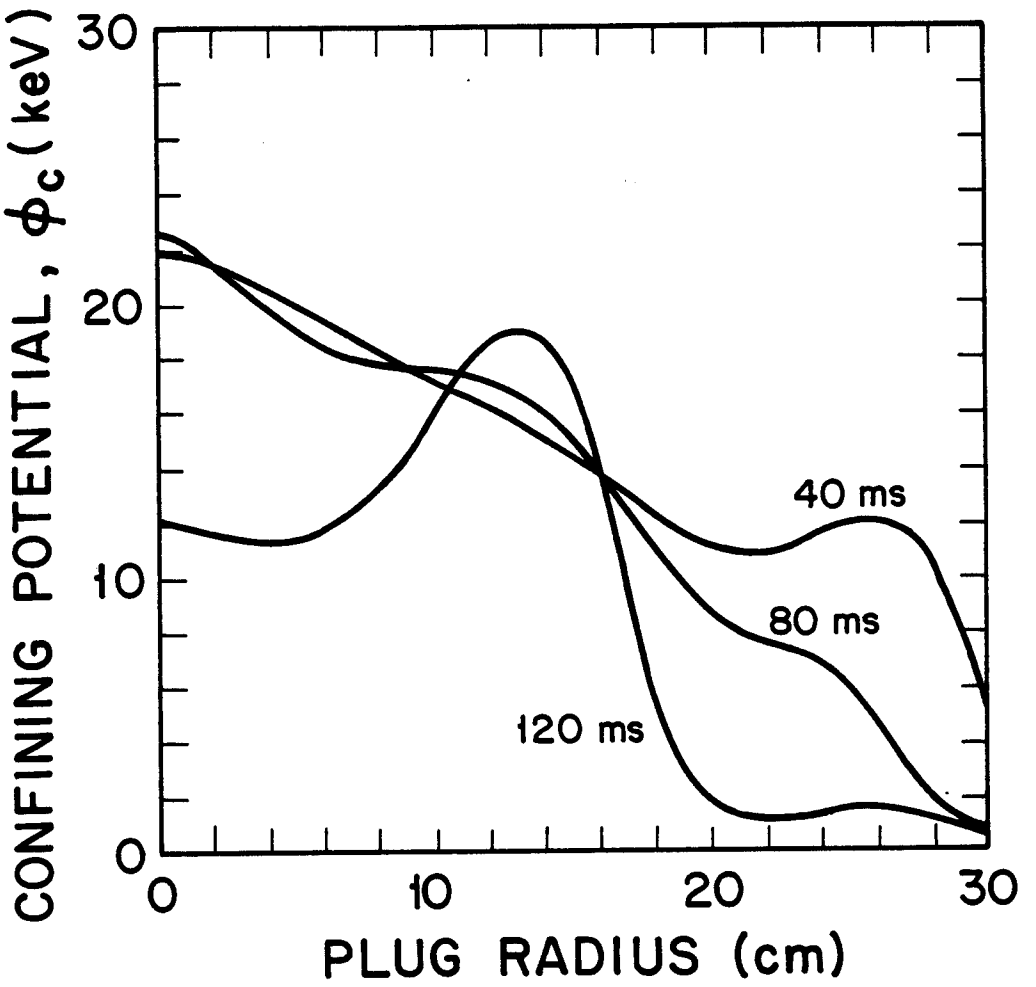

Fig. 27. Radial plots of the plug confining potential for a startup simulation using the ECRH power levels of Table 3.

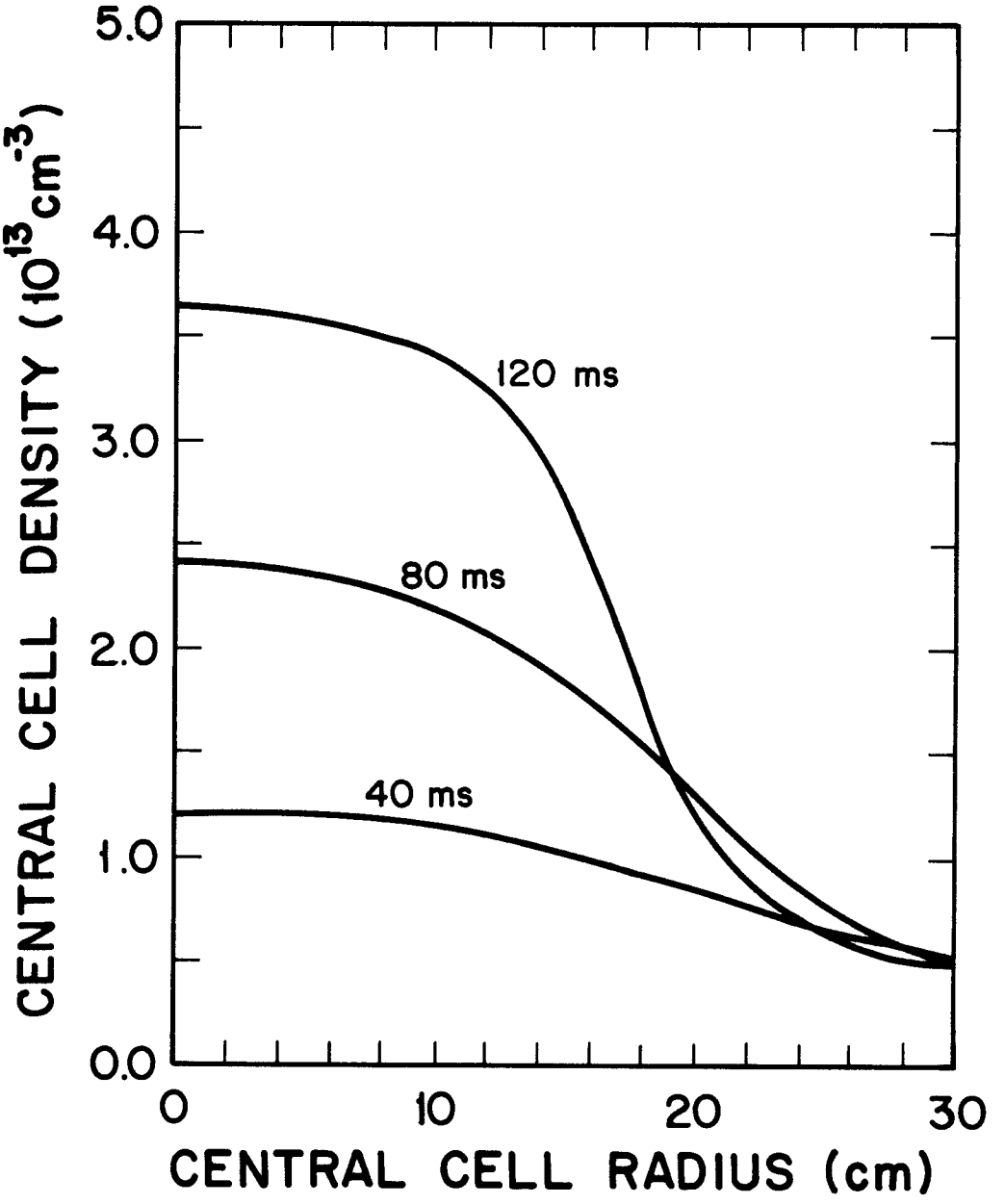

Fig. 28. Radial plots of the central cell density for a startup simulation using the ECRH power levels of Table 3.

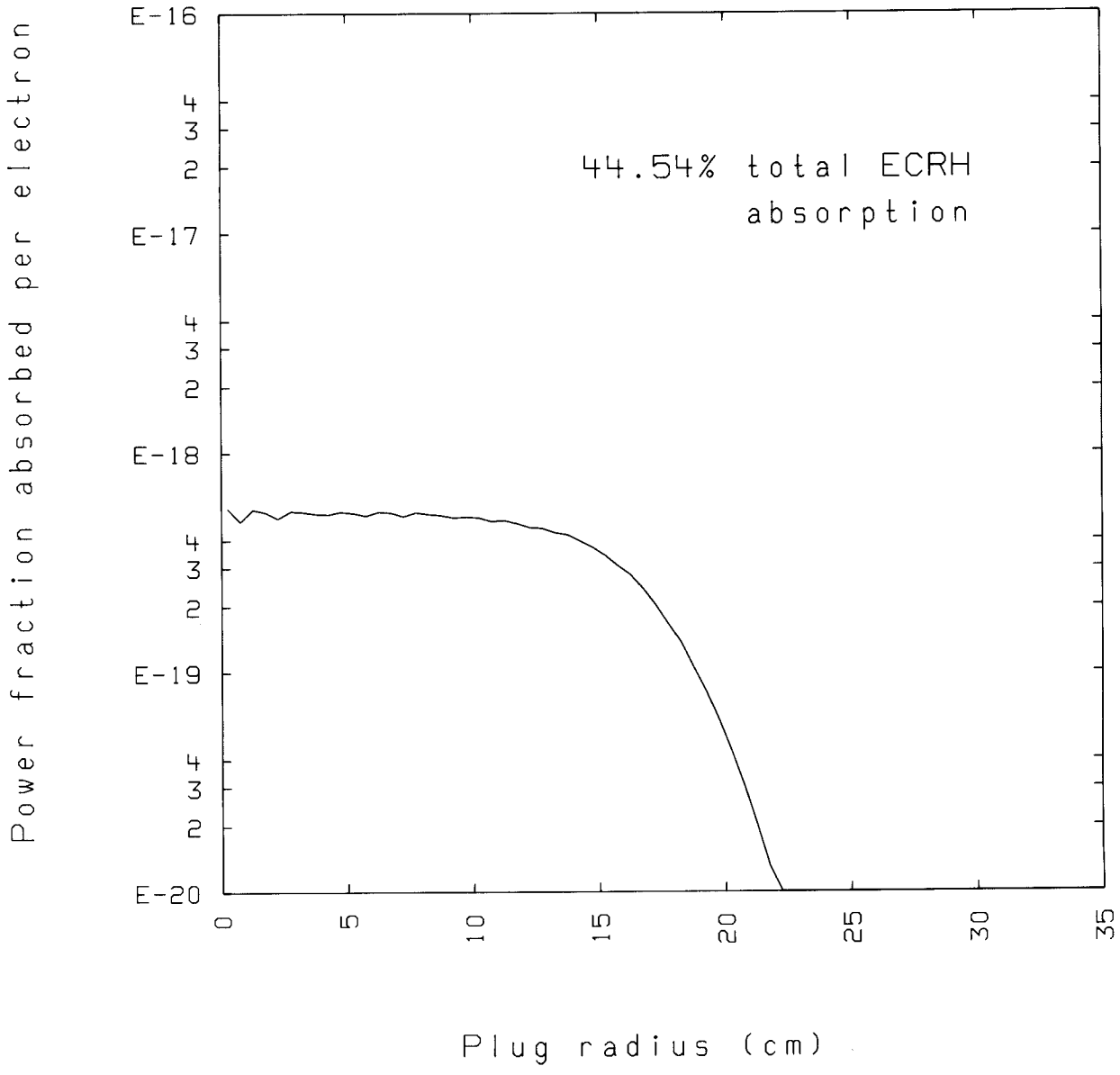

Fig. 29. The fraction of ECRH power absorbed per electron as a function of radius at the 40 ms point of the simulation described in Figs. 24-28.

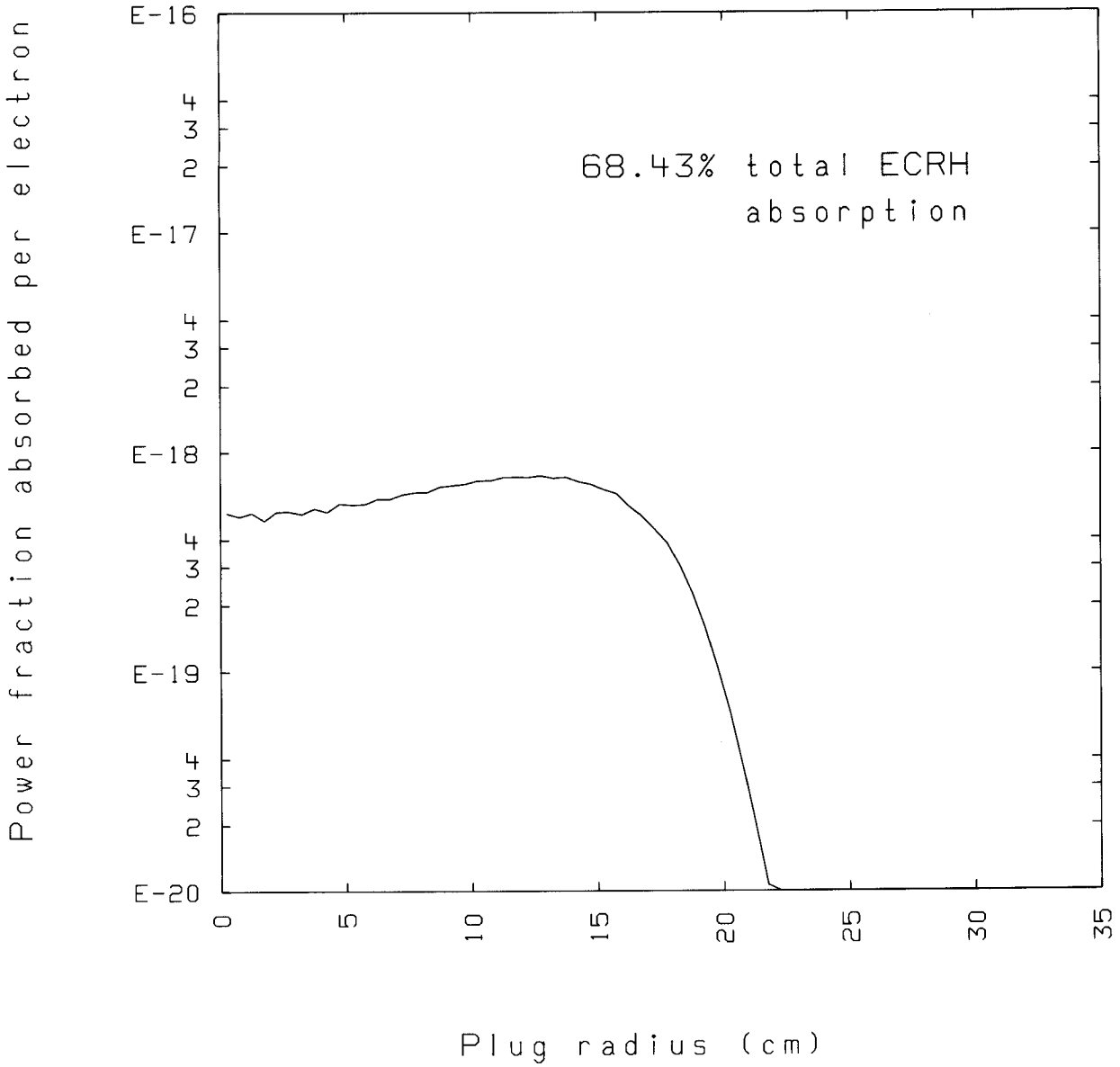

Fig. 30. The fraction of ECRH power absorbed per electron as a function of radius at the 80 ms point of the simulation described in Figs. 24-28.

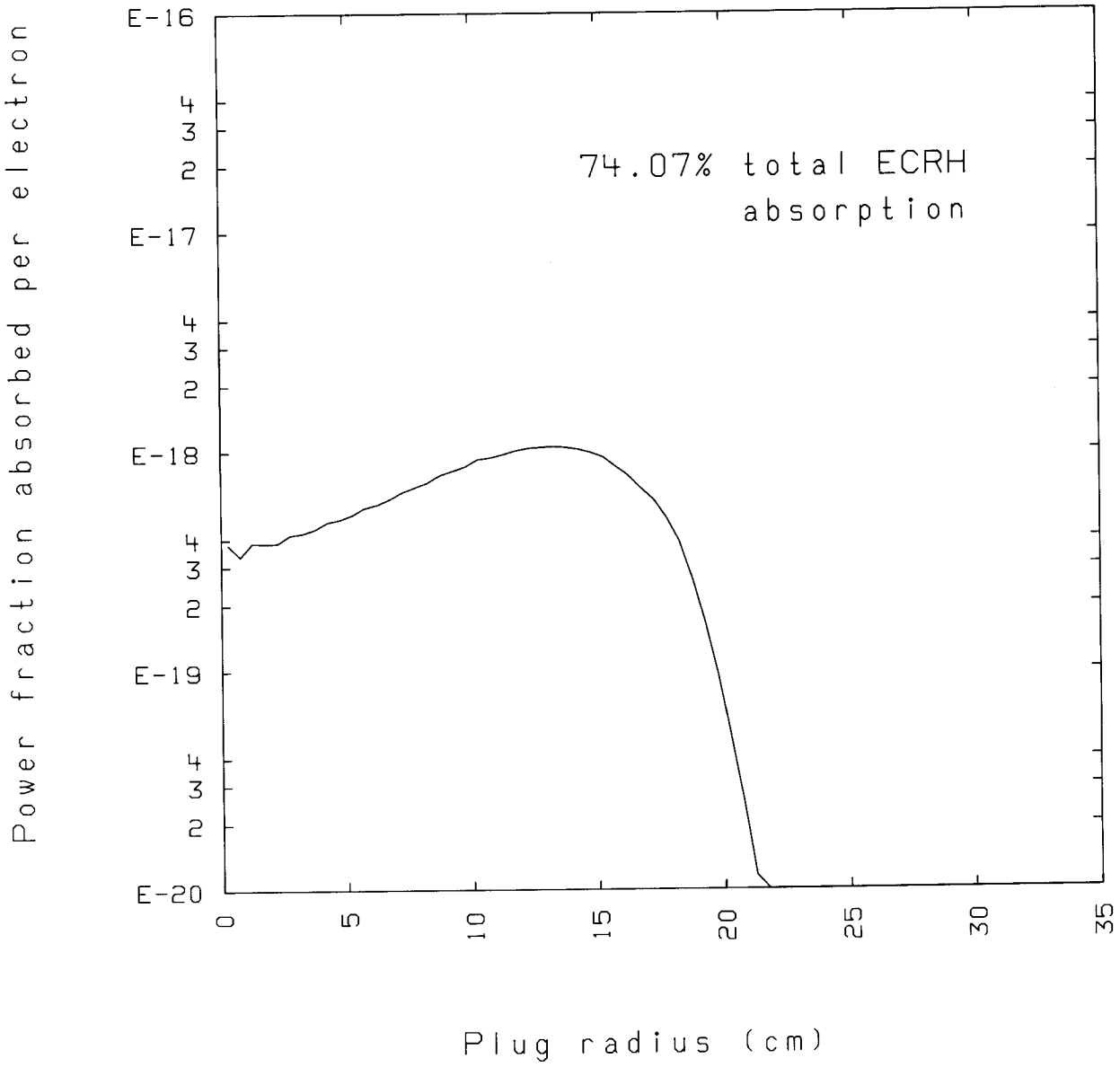

Fig. 31. The fraction of ECRH power absorbed per electron as a function of radius at the 120 ms point of the simulation described in Figs. 24-28.

Although stochastic temperature limits on wave heated electrons exist,[16] for large devices such as TASKA these limits are out of the non-relativistic electron energy regime. The feedback mechanism then continues and the simulation results in a ring of electrons with relativistic energies near the plasma edge, instead of the spatially uniform distribution of plug electrons with a temperature of 59 keV, as desired at equilibrium. The problem in this startup scenario is that we are constrained to use one ECRH launching system, and therefore we are forced to find, for successful operation, a single launch trajectory that will have a spatial absorption of power such that the electron energy losses are nearly balanced, in each radial zone, at all times in the plasma evolution. It is clear that such a trajectory is unlikely to exist. Furthermore, the large amounts of power that must be in this single launch system soon drive any local energy imbalance and temperature rise to a sharp local temperature peak via the feedback mechanism described. The simulations performed here strongly suggest that for the large amounts of ECRH power to be deposited in a plasma that produce spatially uniform electron temperatures, multiple, spatially separated sources must be used so that the power deposited may be radially varied to match the local plasma conditions.

Finally, we present in Figs. 32 and 33 the radial ECRH power deposition profiles for the launch point of the last simulation, assuming Gaussian electron temperature profiles with peaks of 20 and 30 keV respectively. Taken by themselves, the broad, flat profiles may indicate that ECRH heating a bulk plasma to these temperatures, and beyond, is quite simple. We have shown in the above that heating to such temperatures with this system is in fact quite

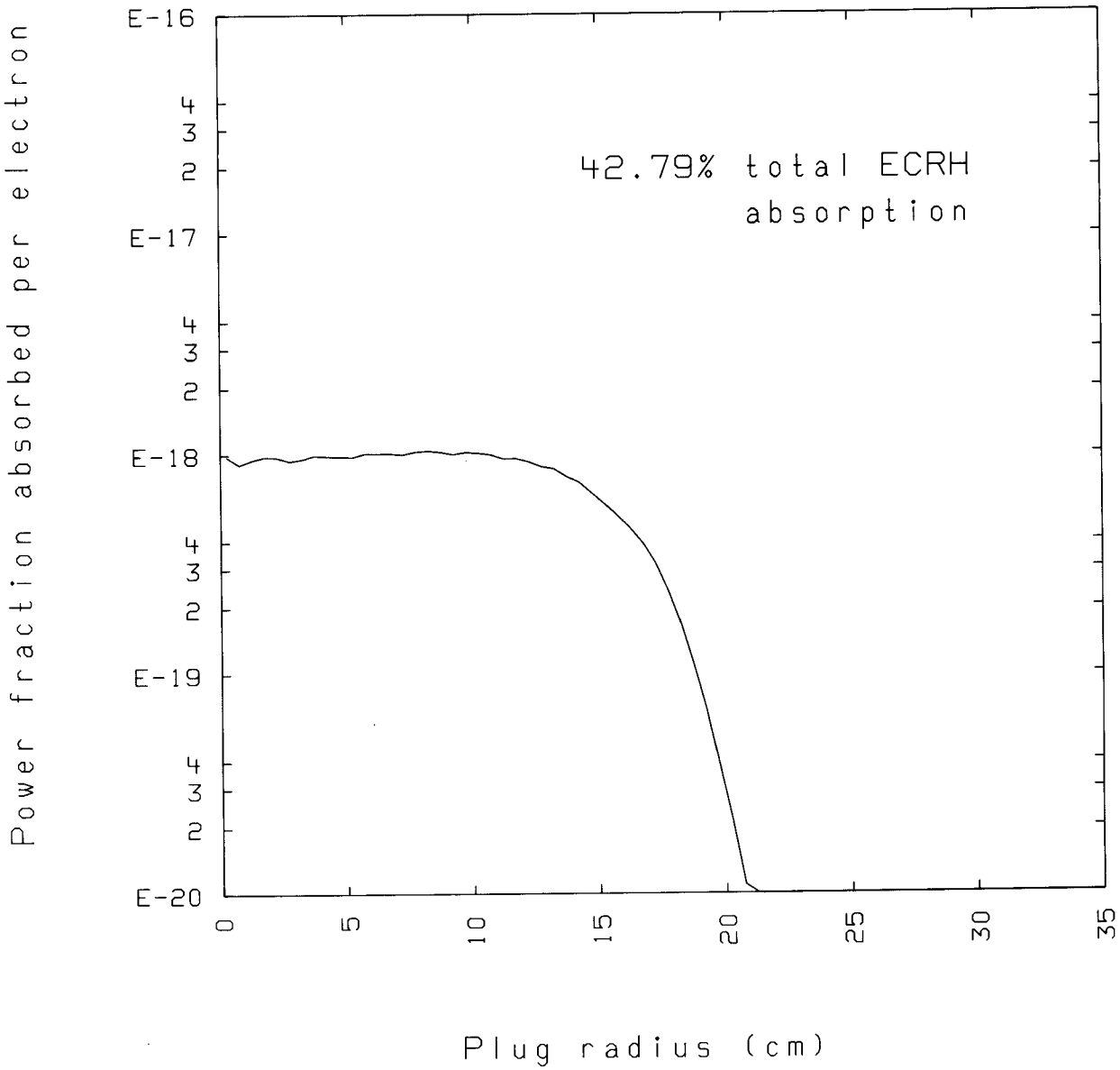

Fig. 32. The fraction of ECRH power absorbed per electron as a function of radius for a plasma with a density of 2 x 10^{13} cm^{-3} and an electron temperature of 20 keV.

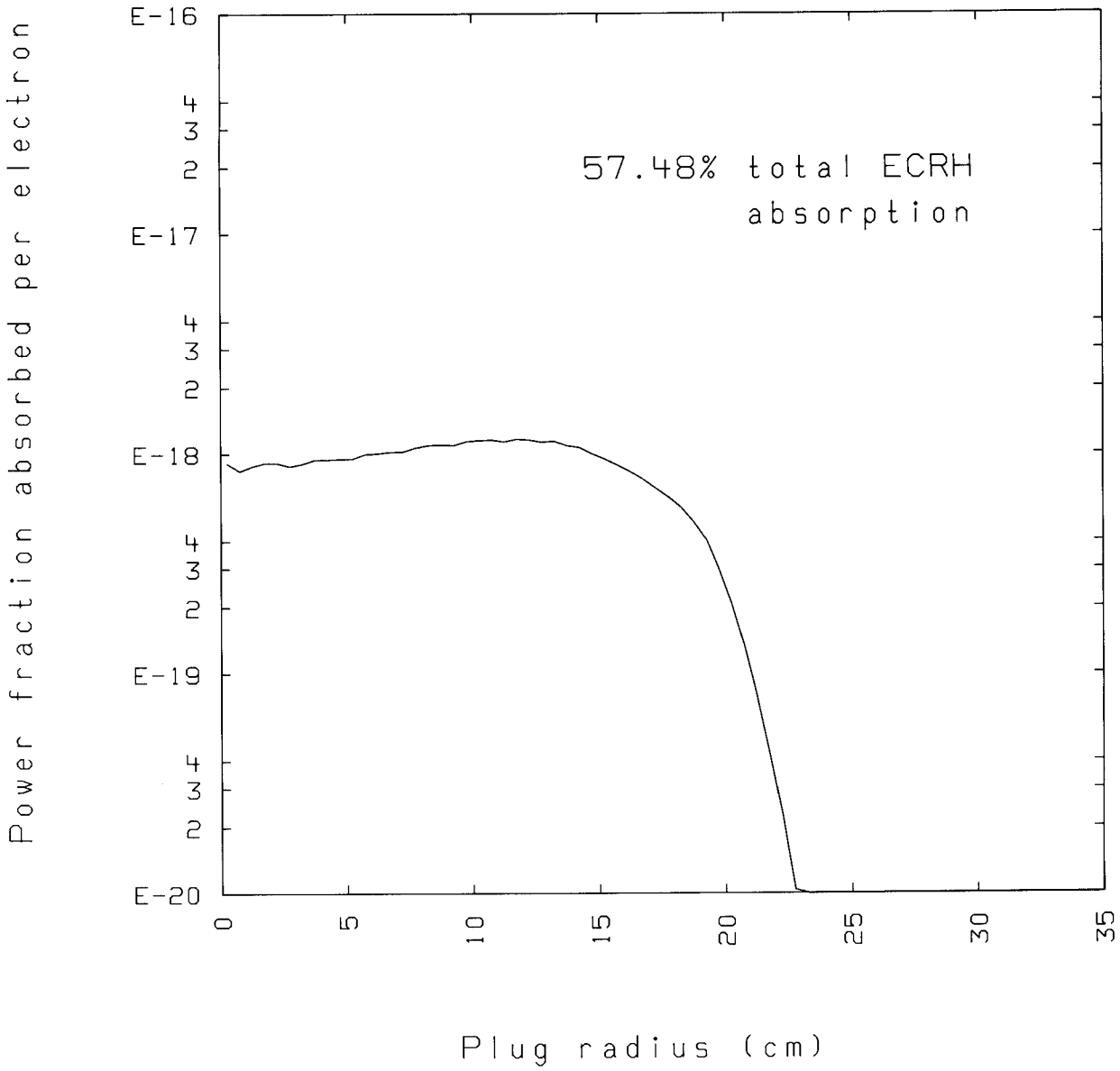

Fig. 33. The fraction of ECRH power absorbed per electron as a function of radius for a plasma with a density of 2 x 10^{13} cm^{-3} and an electron temperature of 30 keV.

difficult, and shown the need for self-consistent calculations of plasma parameters and ECRH absorption to predict spatial heating during plasma startup.

V. Summary

We have described a mechanism developed to link a 3-dimensional ECRH ray tracing-absorption code to a 1-dimensional tandem mirror transport code. The technique expands radial temperature and density profiles along flux surfaces which can accurately simulate the 3-dimensional plasma behavior in a tandem mirror. Along the calculated ray trajectory, the power deposited on these flux surfaces can then be used to create radial absorption profiles for use in the transport code. Simulations may then be performed where the plasma parameters change as a result of the ECRH absorption profiles, and vice versa, so that the plasma's evolution is assured of being self-consistent.

We have also illustrated how using a single ray containing the entire ECRH system's power to model heating will produce singularities in the radial power deposition profile. The power must be distributed among multiple rays to accurately model the spatial extent of a system's ECRH heating, and we have developed a technique for constructing many artificial rays from a single ray tracing-absorption calculation. In this way computing time is minimized.

Finally, we have used the above methods to model the ECRH heating of plug electrons in TASKA startup simulations. We have shown the necessity of plug ECRH during startup, and the difficulty of maintaining a heated electron population using a single launch system. For large injected powers, a feedback mechanism between rising electron temperatures and lower collisional energy losses with greater ECRH power absorption, creates large electron temperature peaks near the plasma edge. These peaks reduce the ECRH power transmitted to the center of the plasma, producing hollow electron temperature profiles.

More study is needed to overcome this positive feedback effect, possibly using multiple ECRH sources to adjust the radial power deposition profile as plasma conditions warrant.

Acknowledgments

The authors would like to acknowledge helpful discussions with Drs. John Santarius and Karl Audenaerde.

References

1. F.H. Coensgen et al., "TMX Upgrade Major Project Proposal," Lawrence Livermore Laboratory Report, LLL-PROP-172 (1980).

2. "Physics Basis for MFTF-B," edited by D.E. Baldwin, B.G. Logan, T.C. Simonen, Lawrence Livermore Laboratory Report, UCID-18496 (1980).

3. B. Badger et al., "WITAMIR-I, A Tandem Mirror Reactor Study," University of Wisconsin Fusion Engineering Program Report UWFDM-400 (1980).

4. B. Badger et al., "TASKA, A Tandem Mirror Fusion Engineering Test Facility," University of Wisconsin Fusion Engineering Program Report UWFDM-500 (1982).

5. K. Audenaerde and J.E. Scharer, "Electron Cyclotron Heating in Weakly Relativistic, Finite-Beta Tandem Mirror Plasmas," University of Wisconsin Fusion Engineering Program Report UWFDM-459 (1982).

6. D.D. Ryutov and G.V. Stupakov, "Diffusion of Resonance Particles in Ambipolar Plasma Traps," Sov. Phys. Dokl. 23, 412 (1978).

7. R.H. Cohen et al., "Collisional Loss of Electrostatically Confined Species in a Magnetic Mirror," Nucl. Fusion 18, 9 (1978).

8. B.G. Logan et al., "An Analytic Model for Classical Ion Confinement in Tandem Mirror Plugs," Nucl. Fusion 20, 12 (1980).

9. J.M. Gilmore, Ph.D. Thesis, University of Wisconsin (1980).

10. M. Abramowitz and J.A. Stegum, "Handbook of Mathematical Functions," U.S. Dept. of Commerce, Washington, D.C. (1972).

11. X.Z. Li and G.A. Emmert, "The DT Fuel Density in the Thermal Barrier of a Tandem Mirror Reactor," University of Wisconsin Fusion Engineering Program Report UWFDM-419 (1981).

12. D.E. Baldwin and B.G. Logan, Phy. Rev. Lett. 43, 1318 (1979).

13. R.H. Cohen, Nucl. Fusion 20, 1421 (1980).

14. "NRL Plasma Formulary," David L. Book ed., Naval Research Laboratory, Washington, D.C. (1980).

15. S. Tamor, "A Simple Fast Routine for Computation of Energy Transport by Synchrotron in Tokamaks and Similar Geometries," Science Applications Inc. Report SAI-023-81-189-LJ, LAPS-72 (June 1981).

16. T.D. Rognlien, "Frequency Splitting and Collisional Decoupling for Removing Superadiabatic Barriers in ECRH Experiments," Lawrence Livermore Laboratory Report UCRL-87519 (April 1982).